Quaternary Science Advances 13 (2024) 100134

Contents lists available at ScienceDirect

Quaternary Science Advances

journal homepage: www.sciencedirect.com/journal/quaternary-science-advances

Abrupt and persistent shutdown of the thermohaline forcing during MIS5e in the Adriatic Sea: Insights from shallow-water sapropel sediments

T. Tesi [a,*], A. Asioli [b], E. Previde Massara [c], P. Montagna [a], C. Pellegrini [b], A. Nogarotto [a,d], A. Cipriani [e], A. Piva [c], F. Muschitiello [f], M. Rovere [b], P. Viaggi [c], F. Trincardi [g]

[a] Istituto di Scienze Polari - Consiglio Nazionale delle Ricerche ISP-CNR, 40129, Bologna, Italy
[b] Istituto di Scienze Marine - Consiglio Nazionale delle Ricerche ISMAR-CNR, 40129, Bologna, Italy
[c] Eni S.p.A. Upstream Research and Technological Innovation, 20097, San Donato Milanese, MI, Italy
[d] Campus Scientifico, Università Ca' Foscari Venezia, 30172, Venezia Mestre, VE, Italy
[e] Dipartimento di Scienze Chimiche e Geologiche Università di Modena e Reggio Emilia, 41125, Modena, Italy
[f] Department of Geography - University of Cambridge, Cambridge, CB2 3EN, UK
[g] Dipartimento di Scienze del Sistema Terra e Tecnologie per l'Ambiente, CNR, P.le Aldo Moro 7, Roma, Italy

ARTICLE INFO

Keywords:
Deoxygenation
Sapropel
Thermohaline circulation

ABSTRACT

During the Quaternary, the Eastern Mediterranean Sea (EMS) experienced cyclical events of stagnation driven by natural climate variability. The resulting deoxygenation left well-preserved evidence in the sedimentary record as organic carbon-rich deposits referred to as sapropels. Although drastic modifications in the degree of dense-water formation over the EMS shelves exerted first-order control on the deoxygenation, most of the focus has been traditionally placed on the deep EMS. To provide a shallow-water perspective, here we investigated the sapropel S5 in the Adriatic shelf (borehole PRAD1-2) deposited during MIS5e (129-116 ka). This archive is strategically located in a region where the Northern Adriatic Dense Water (NAdDW) interacts with the seabed before cascading across the continental slope. We used Zr/Rb and MgO/Al_2O_3 to assess bottom current energy and north-to-south sediment transport dynamics, both regulated by the changes in NAdDW production intensity. In addition, we used stable isotopes ($\delta^{13}C$ and $\delta^{18}O$) of foraminifera, redox sensitive elements (U, Mo and Sb), foraminifera assemblages as well as alkenones to reconstruct the paleo-environmental conditions during the S5 formation.

Our study provides an unprecedented reconstruction of the physical forcing controlling the deoxygenation during the S5 formation. Results reveal that the shutdown of the NAdDW occurred in a few centuries (0.67 ± 0.22 kyrs), when freshening of surface waters combined with warming of winter temperatures mutually hampered the dense water formation. A few centuries after the NAdDW shutdown, the Adriatic shelf experienced euxinic waters for about 2 kyrs followed by a progressive reoxygenation that lasted 4 kyrs. We explain this second phase as a general recovery driven by increased surface salinity over the EMS combined with winter cooling. This favoured surface water mixing without, however, producing dense water in the Northern Adriatic and thus collectively the interruption of the dense water production lasted for 6 kyrs since the onset of MIS5e. Overall, our finding highlights that the thermohaline forcing responded to climate change much quicker than inferred by earlier studies that suggested instead a millennial-scale prelude necessary to develop stagnation. In addition, our results provide solid evidence about the large-scale impact of the deoxygenation during S5 that is capable of invading the continental shelf. Comparison with the latest regional models illustrates how none of the future simulations covering different climate change scenarios reproduces an event over the EMS margins comparable with what described in this study.

* Corresponding author.
E-mail address: tommaso.tesi@cnr.it (T. Tesi).

https://doi.org/10.1016/j.qsa.2023.100134
Received 12 June 2023; Received in revised form 9 October 2023; Accepted 10 October 2023
Available online 16 October 2023

1. Introduction

Since the 1950s, the ocean interior has globally lost about 2% of its dissolved oxygen and by 2100 Earth System Models predict a further decline by up to 7% (Schmidtko et al., 2017). Human-induced climate change has been playing a central role because ocean warming acts by reducing both oxygen dissolution and deep ventilation (Kwiatkowski et al., 2020; Reale et al., 2022). At regional level, the future loss of dissolved oxygen in a warming Mediterranean Sea remains still highly elusive because different climate simulations generate contrasting deep-water convection scenarios and this inevitably hampers our ability to predict the evolution of dissolved oxygen (Adloff et al., 2015; Herrmann et al., 2008; Somot et al., 2006; Vilibić et al., 2013). Acknowledging this uncertainty, Powley et al. (2016) has recently modelled upper and lower boundaries of the anticipated deoxygenation for the Mediterranean Sea according to different scenarios. Their study highlights that convection has a central role despite being highly uncertain. Another relevant outcome from Powley et al. study is the fact that, when convection is highly reduced, anoxia takes place only after centuries since the onset of stagnation and it is mainly confined in the deep Eastern Mediterranean Sea (EMS). Overall, while severe deoxygenation seems unlikely by the end of the 21st century in all different simulation scenarios, understanding the centennial-scale variability of dissolved oxygen emerges as a fundamental aspect needed to assess the long-term effect of reduced ventilation on the Mediterranean ecosystem services and plan appropriate mitigation actions.

In this respect, the cyclical deposition of organic carbon-rich sediments in the Mediterranean Sea, known as sapropels, represents an ideal example of long-term deoxygenation driven by climate change (Grant et al., 2022; Rohling et al., 2015; Rossignol-Strick et al., 1982). However, sapropels do not represent *per se* analogous of the future climate change as the driving mechanisms behind the weakening of the dense water formation differ in many aspects. Yet, sapropels can provide crucial information about the centennial-scale relationship between ventilation and deoxygenation and put the future evolution of the Mediterranean Sea into a broad context of natural climate variability.

A survey of the current literature reveals, however, that most of the studies dealing with sapropelite beds primarily focused on the effect of stagnation to infer changes in the deep-water formation rather than resolving the convection in the first place (Rohling et al., 2015). In fact, previous studies traditionally focused on deep sediments where the deoxygenation event is indeed well-expressed but disconnected from the shelves where the dense water forms. To provide a shallow-water perspective, here we investigated the sapropel S5 anoxic event occurred during the Last Interglacial (MIS5e) in the Adriatic Sea. The sedimentary archive analysed in this study (borehole PRAD1-2; Piva et al., 2008b; Ridente et al., 2009, 2008) was collected at the edge of the Mid-Adriatic Depression at 185.5 m water depth (Figs. 1 and 2). Here, the dense plume interacts with the seabed prior to cascading off the margin further south where it supplies oxygen to the deep EMS (Bonaldo et al., 2016; Chiggiato et al., 2016; Janeković et al., 2014; Langone et al., 2016; Marini et al., 2016).

In addition to its strategic location, the unique characteristic of shallow-water sapropelite beds preserved in PRAD1-2 lays on the fact that these sediments recorded both the physical forcing and the biological/geochemical evidence of stagnation (Piva et al., 2008a). Thus,

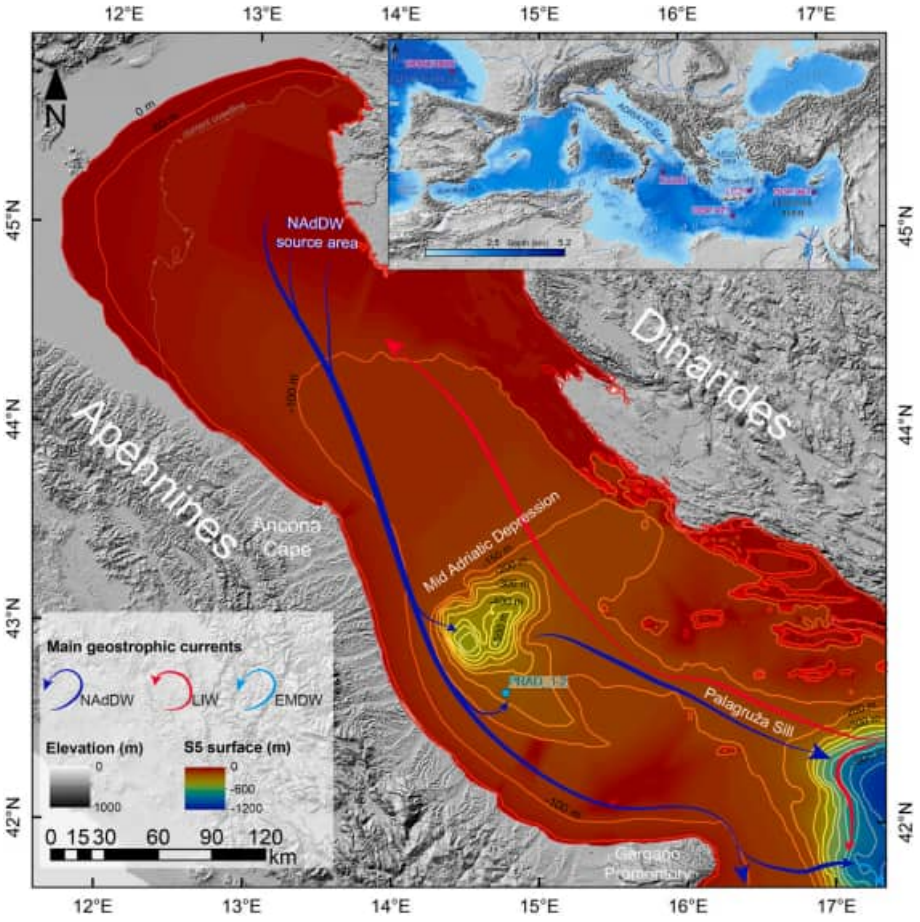

Fig. 1. Map of the study area. (a) The inset shows the location of PRAD1-2, MD04-2845 (Salonen et al., 2021; Salonen et al., 2021), LC21, ODP971A, KS205 and ODP967 (Amies et al., 2019; Cane et al., 2002; Grant et al., 2012). (b) Dark blue arrows show the path of the Northern Adriatic Deep Water (NAdDW) while the red arrows and the light blue arrows display the Levantine Intermediate Water (LIW) and Eastern Mediterranean Deep Water (EMDW), respectively.

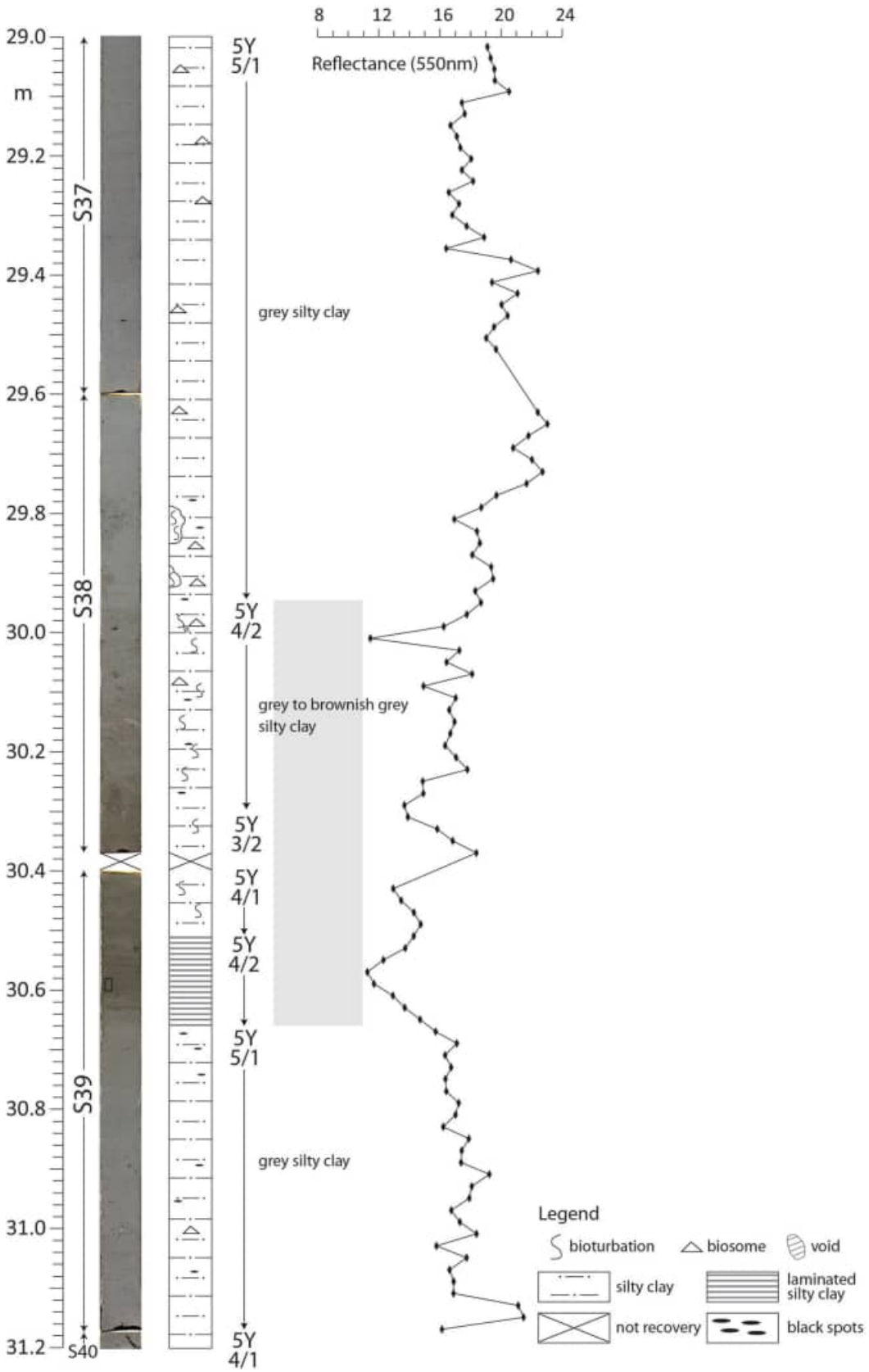

Fig. 2. Photo and visual description of the investigated PRAD1-2 borehole interval. Colors are reported according to the Munsell table. The vertical grey bar represents the lithological boundaries of the sapropel S5 (i.e., 30.66–29.95 m). On the right the reflectance as quantitative expression of the chromatic changes (after Piva et al., 2008a): low and high values indicate dark and light sediment, respectively. On the picture is also reported the position of the thin section discussed in the text (30.58–30.60 m).

even considering the inevitable age uncertainty that affects any archive, the sequence of (physical, chemical and biological) events are stratigraphically respected throughout our record. This, ultimately, allows a robust interpretation of timing constraints among distinctive processes in place. Another important benefit with studying shallow sapropels is the opportunity to resolve the regional-scale expression of an anoxic event and reveal possible leads and lags between shallow and deep systems. In this respect, we synchronised our record from the shelf with the LC21 sediment core from the deep Aegean Sea to harmonise shallow-water and deep-water archives over a common time scale (Amies et al., 2019; Grant et al., 2012).

The overarching goal of this study was to shed new insights into the bond that ties together dense water formation over the shelf with shallow-water deoxygenation. We focused on sapropel S5 (MIS5e) because this is one of the most severe anoxic events of the late Quaternary (Capotondi et al., 2006; Grant et al., 2022; Marino et al., 2007; Schmiedl et al., 2003) and, thus, it defines in first-order approximation, the upper boundary of a natural deoxygenation event. We then compared our historical perspective with the anticipated deoxygenation scenarios gained from regional models to evaluate the impact of future deoxygenation of the Mediterranean Sea within a framework of natural climate variability.

2. Background

2.1. PRAD1-2 borehole and study region

The EU-funded PROMESS1 project ("PROfiles across MEditerranean Sedimentary Systems") was the first ever attempt to drill through Mediterranean margins to obtain very expanded and continuous Quaternary marine records during the last 500 ka. The 71.2 m long PRAD1-2 borehole was drilled southern flank of the Mid-Adriatic Depression at 185.5 m water depth (42°40′34.7″N, 14°46′13.5″E; Fig. 1). The record spans between the late MIS11 and MIS1 (ca. the last 370 kyrs) (Bourne et al., 2015; Piva et al., 2008b), and allows paleoenvironment reconstructions at centennial time-scale (Pellegrini et al., 2017). In this study, we focused on a 20-kyr-long interval that goes from MIS6 to MIS5d (ca. 136-116 ka BP) corresponding to section S38 and S39 of PRAD1-2 (Fig. 2).

The study area is seasonally bathed by the Northern Adriatic Dense Water (NAdDW) (Marini et al., 2016). This water mass is associated with cold and dry Bora wind in winters that results in a severe heat loss in the Northern Adriatic region (Janeković et al., 2014). The newly formed dense plume rich in oxygen, under gravity and Coriolis force, travels southward along the western Adriatic before cascading into the Southern Adriatic basin in early spring (Vilibić and Supić, 2005). Here, the NAdDW merges with the water mass generated by open-water convection to form the Eastern Mediterranean Deep Water that ventilates and oxygenates the deep EMS (Bensi et al., 2013).

Taking into consideration tectonic uplift, compaction and eustatic variability at the PRAD1-2 site, Maselli et al. (2010) suggested a paleo-water depth of ca. 180 m during MIS5e which was then confirmed by foraminiferal associations that indicate a paleo-environment compatible with a bathymetry range between 120 and 200 m water depth. In Fig. 1, we reconstructed the paleo-bathymetry in the Northern and Central Adriatic at the onset of MIS5e by removing the thickness of sediments that are younger than MIS5 based on Pellegrini et al. (2018), and considering coast line position during the last interlgacial sea level high stand (Ferranti et al., 2006). The obtained bathymetry chart fits with the overall paleo depth suggested by Maselli et al. (2010) and provides the general physiographic setting of the Adriatic shelf during MIS5e.

3. Methods

3.1. Foraminfera and stable isotopes ($\delta^{13}C$ and $\delta^{18}O$)

Quantitative analysis of planktic and benthic foraminifera was performed on 1-cm thick sediment intervals. Sediment were oven dried at 50 °C, washed through a 0.063 mm sieve, and dried at 50 °C. Each sample was split into aliquots and entire aliquots were counted to reach at least 300 specimens of planktic foraminifers and 300 specimens of benthic foraminifers. Samples with the total number of foraminifera <300 were completely counted. The fraction >0.106 mm was examined, excluding juvenile, encrusted, filled specimens. *Globigerinoides ruber* comprises *Globigerinoides ruber* (pink and white varieties) and *Globigerinoides elongatus*, while *Globigerinoides sacculifer* includes *Globigerinoides trilobus*, *Globigerinoides quadrilobatus* and *Globigerinoides sacculifer* according to Schiebel and Hemleben (2017). The adopted taxonomy of planktic foraminifera refers to Schiebel and Hemleben (2017). For the ecological information of planktic foraminifera, in this study we refer to Hernández-Almeida et al. (2011), Mallo et al. (2017), Pujol and Grazzini (1995), Rigual-Hernández et al. (2012), Schiebel and Hemleben (2017) and references therein. For the benthic foraminifera ecological requests we refer to Barmawidjaja et al. (1992), De Rijk et al. (1999), De Stigter et al. (1998), Jorissen (1999, 1988), Murray (2006), Schmiedl et al. (2000), Sen Gupta (2003). Oxygen and carbon stable isotope analyses ($\delta^{18}O$ and $\delta^{13}C$) were carried out on those planktic and benthic species present throughout the core to avoid temporal gaps. Well preserved specimens of planktic (*Globigerina bulloides* and *Globigerinoides ruber alba*) and benthic (*Bulimina* ex gr. *marginata*) foraminifera were picked up from the fraction >0.180 mm. The O and C stable isotope analysis were performed at the Leibniz Laboratory for Radiometric Dating and Stable Isotope Research, Christian Albrechts University, Kiel (Germany), by means of a Kiel IV automated carbonate preparation device, connected to a MAT 253 Finnigan mass spectrometer. The carbon dioxide, obtained after reaction with phosphoric acid under vacuum at −75 °C, was analysed eight times for each sample. The results are expressed as per mil (‰) deviation with respect to the international V-PDB standard. The analytical error is better than 0.05‰ ($\delta^{13}C$) and 0.08‰ ($\delta^{18}O$) based on the performance of international (NBS19, IAEA-603: and laboratory-internal carbonate standards (see also Bulian et al., 2022). Additional $\delta^{18}O$ and $\delta^{13}C$ data of *G. bulloides* and *B. marginata* were available from Piva et al. (2008a) at low resolution. The $\delta^{18}O$ and $\delta^{13}C$ analyses presented in Piva et al. (2008a) were performed in the same laboratory.

3.2. Age-depth model

The stratigraphic correlation within the S5 interval follows the general framework proposed by Cane et al. (2002) and used in other studies (Amies et al., 2019; Capotondi et al., 2006; Marino et al., 2007) that relies on bio- (planktic foraminifera) and isotopic ($\delta^{18}O$ and $\delta^{13}C$) events observed across the EMS within the S5 unit. Figure 3 shows the 11 primary events identified in PRAD1-2 which were then stratigraphically correlated with ODP core 971A (Fig. 1). For the latter record, a LC21-equivalent depth scale was initially generated by Marino et al. (2007) following the same stratigraphic framework developed by Cane et al. (2002). Amies et al. (2019) have then transferred the LC21-equivalent depth scale to the latest LC21 age model that builds on the synchronization of LC21 *G. ruber* $\delta^{18}O$ to the U–Th dated Soreq Cave speleothem $\delta^{18}O$ record (Grant et al., 2012). The reason behind the choice of stratigraphically correlating PRAD1-2 to 971A rather than directly to LC21 lays on the fact that the first two cores display more primary events in common (Fig. 3).

The age-depth model was derived by tuning PRAD1-2 to 971A using the G. ruber $\delta^{18}O$ stratigraphy and the 11 tie-points shown in Fig. 3. By doing so, PRAD1-2 is indirectly synchronised to LC21 within the sapropel unit. The stratigraphic alignment was modelled using an

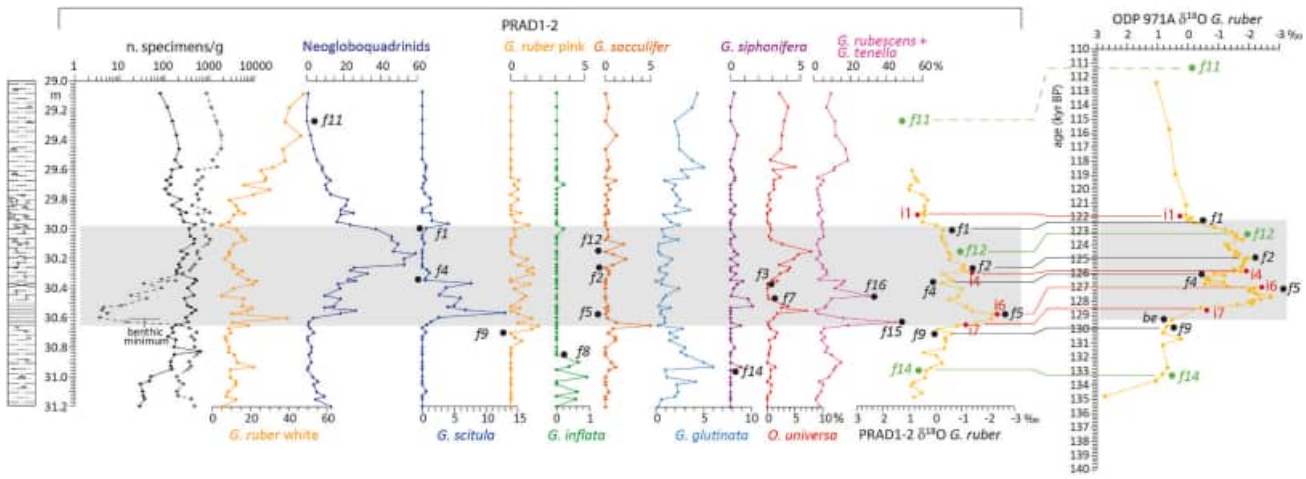

Fig. 3. Distribution of the planktic taxa of PRAD1-2 according to Cane et al. (2002). The figure includes also the concentration of planktic (dark line) and benthic foraminifera (grey line) as well as the sum of *Globoturborotalita rubescens* and *Globigerinoides tenellus*. The faunal correlation markers (letter "*f* ") according to Cane et al. (2002) are reported, except for *Globigerinoides ruber* white and *Globigerinita glutinata* of which we could not identify the bio-events. The primary correlation markers are written in black, while the secondary correlation markers in green. The $\delta^{18}O$ *G. ruber* curve of PRAD1-2 is also reported along with the recognized faunal and isotopic markers (letter "*i* ", in red). On the right hand side, the $\delta^{18}O$ *G. ruber* curve of the reference hole ODP971A is reported vs age (after Amies et al., 2019). The age of the faunal marker f11 has been extrapolated from the youngest two age points available in Amies et al. (2019). The age of the faunal and isotopic markers in 971A curve has been transferred to the PRAD1-2 $\delta^{18}O$ *G. ruber* to obtain 11 control points for the age-depth model. The grey areas indicate the sapropel S5.

automated algorithm based on Markov-chain Monte Carlo (MCMC) inversion. The method was previously presented in Muschitiello et al. (2020) and was successfully applied on a variety of paleoceanographic records (Cutmore et al., 2022; Muschitiello et al., 2019; Sessford et al., 2019). The $\delta^{18}O$ data were used as inputs to the automated alignment algorithm to obtain a continuous synchronization of PRAD1-2 and 971A, whereas the tie points served as gateways to "nudge" the $\delta^{18}O$ alignment assuming an uncertainty in the depth domain constrained by neighbouring $\delta^{18}O$ sample points (with 2σ). The alignment procedure described here hinges on the assumption of direct synchrony of variations in the $\delta^{18}O$ signals at both coring sites. However, it provides a reproducible and continuous alignment that accounts for potential uneven compaction/expansion of sediment cores. The algorithm was run for 10^6 iterations after discarding the initial 10^5 MCMC samples ("burn-in"). The median of the MCMC alignment sample was used to derive the posterior optimal syncrhonization between core PRAD1-2 and 971A, while the variability of the sample was used to estimate the posterior uncertainty of the alignment.

3.3. Inorganic geochemistry

Major and minor elements were determined by X-ray fuorescence (XRF) on pressed pellets (Leoni and Saitta, 1976; Rivalenti et al., 2004) using a Philips PW 1480 wavelength-dispersive spectrometer housed at the Department of Chemical and Geological Sciences of the University of Modena and Reggio Emilia (UNIMORE). For this study we report only Al_2O_3, MgO, Zr and Rb concentrations. Data are reported as weight percent (%) and μg/g for major and minor elements, respectively. Uncertainties of XRF, expressed as relative standard deviation in percentage, are considered accurate within 2–5% for major elements and lower than 10% for minor elements based on replicate analyses of reference materials.

Molybdenum (Mo), uranium (U), antimony (Sb) and titanium (Ti) concentrations were quantified via ICP-MS analyses. Briefly, about 50 mg of the sediment samples were digested with a MARS 6 (CEM Corp., Kamp Lintfort, Germany) microwave system following Zimmermann et al. (2020). Digestion took place at 180 °C for 300 min into 20 mL pre-cleaned TFM digestion vessels using the following acid mixtures: 4 mL HNO_3 (65% w/w Suprapur), 2 mL HCl (30% w/w Suprapur) and 2 mL HBF_4 (38% w/w ultra pure). The digestate solutions were then transferred to acid-clean Falcon tubes, dried down under fume hood on a hot-plate and then re-dissolved in 3M HNO_3 and MilliQ water to a final HNO_3 concentration of 4% w/w. Trace elements were measured using a quadrupole ICP-MS (Thermo Fisher Scientific, XSeriesII), equipped with a collision–reaction cell and a CETAC ASX 520 autosampler housed at the Centro Interdipartimentale Grandi Strumenti of UNIMORE (Argentino et al., 2019). $A^{115}In$ solution was employed as internal standard. Calibration curves were obtained using multi-element standards (IVICP-MS-71A and 71B, Inorganic Venture), in the range of 1–1000 ppb. Replicate measurements (n = 3) on each sample solution provided precision RSD overall better than 5%.

To account for the contributions of detrital minerals, redox-sensitive elements (RSE) were normalized to Ti by calculating Enrichment Factors (EFs) for Mo, U and Sb ($RSE_{EF} = (RSE/Ti)_{sample}/(RSE/Ti)_{detrital}$. Detrital values were based on the average of 10 samples that define the mean background value (Chiu et al., 2022; Clarkson et al., 2021). This type of normalization circumvents the bias given by the detrital input in a shallow-water setting proximal to river outlets like our study region. Data are also reported in the Supplementary section as μg/g values and normalized to Ti.

3.4. Organic geochemistry

Freeze-dried samples were powdered and homogenized in an agate mortar. About 20 mg of acidified sediments (1.5 M HCl) were analysed using a Thermo Fisher Elemental Analyser (FLASH, 2000 CHNS/O) for total organic carbon concentration (TOC, wt.%) (Pellegrini et al., 2021).

An aliquot of freeze-dried sediments (ca. 1 g) was transferred into pre-combusted vials. A known amount of docosane (internal standard) was added followed by addition of a solvent mixture (dichloromethane: methanol (DCM:MeOH), 9:1, v/v). Samples were sonicated (15 min at 60 °C), centrifuged and the supernatant was transferred in pre-combusted vials. Extraction steps were repeated two more times. Saponification of dry extracts was carried out using 5% methanolic potassium hydroxide at 70 °C for 1h. The neutral fraction was extracted 3 times with hexane (Hex). Extracts were dried (N_2 stream) and re-dissolved in 500 μl of Hex:DCM (3:2, v/v) prior to purification via silica gel column chromatography. The apolar fraction was eluted with Hex:DCM (3:2, v/v) and the polar fraction with MeOH:DCM (1:1, v/v). The acid fraction was recovered after acidifying the leftover extract with

ethyl acetate (Tesi et al., 2021).

In this study, we used the method developed by Rontani et al. (2011) for quantifying alkenones via GC-MS. Briefly, the apolar fraction was re-dissolved in a methyl tert-butyl ether/methanol mixture (3:1, v/v) with $NaBD_4$ for the conversion of alkenones to alkenols. Excess $NaBD_4$ was neutralized with an aqueous solution of NH_4Cl followed by acidification with HCl and extraction with Hex:DCM (4:1, v/v). Reduced extracts were dried (N_2 stream), redissolved in pyridine and derivatised with bis-trimethylsilyl-trifluoroacetamide for GC-MS analyses.

Alkenones were analysed using an Agilent 7820A chromatograph fitted with a J&W DB5-MS column (30 m length, 0.25 mm ID, 0.25 mm film thickness) coupled to a 5977BMSD. The oven temperature ramp was programmed from 60 to 300 °C at 10 °C/min (hold time 10 min). The detector was operated in both Selective Ion Monitoring (SIM) and SCAN modes. Di-, tri- and tetra-unsaturated C_{37} methyl ketones were quantified integrating the peaks of ion *m/z* 118 in SIM mode. Correction factors (conversion of SIM to SCAN areas) were obtained injecting purified amounts of reduced alkenones. Corrected areas were used to calculate the UK'_{37} index as follow:

$$UK'^{k}_{37} = \left(\frac{C37:2\,Me}{C37:2\,Me + C37:3\,Me}\right)$$

For comparison with previous studies (Marino et al., 2007), UK'37 index was converted in Sea Surface Temperature (SST) using the equation presented in Müller et al. (1998).

3.5. Thin section

A sample, corresponding to the darkest and laminated unit within the sapropel deposit, was selected for Scanning Electron Microscope (SEM) (Fig. 2). The sample was stabilized with Spurr resin after removal of pore water with acetone (Schimmelmann et al., 2015), and ion-milled into a Gatan 600 DuoMillTM (an ion mill originally designed for preparation of Transmission Electron Microscopy specimens, Schieber, 2013). This results in a gentle polishing and produces smooth surfaces. The same method was successfully tested to study primary sedimentary structures and organic matter in modern Adriatic samples (Pellegrini et al., 2021).

4. Results

4.1. Foraminifera

The foraminiferal distribution in the investigated sequence defined at least three main domains (Figs. 2 and 3) corresponding to different phases of S5 deposition. In the lower one, up to the base of the sapropel unit (m 30.66), benthic foraminifera were abundant, while planktic foraminifera, scarce at the base, increased in concentration upward by one order of magnitude. Planktic foraminifera were dominated by *T. quinqueloba*, and *G. bulloides*, followed by *G. ruber* white and *G. glutinata*, while *G. inflata* was scattered and not frequent. In the second sediment interval (dark sediments, Fig. 2), the lowermost part, corresponding to the laminated phase, showed benthic foraminifera concentration decreasing two orders of magnitude reaching a minimum in the laminated unit (Fig. 3). During this phase, benthic taxa such as *Globobulimina* spp (deep infaunal) and Bolivina spp, dominated the assemblage. This phase recorded also, at its base, the abrupt increase of *G. rubescens* and *G. tenella*, and of *G. sacculifer*, followed, in sequence, by the strong increase of *G. scitula* and the progressive increase of neogloboquadrinids, this later culminating in the late phase of the Sapropel deposition. The third interval (post sapropel deposition) revealed an opposite trends in the distribution of neogloboquadrinids and *G. ruber* with the former decreased while the latter increasd. Other taxa, such as *G. scitula*, after showing a sharp drop within the sapropel unit, increased again just after the end of the S5, while *G. inflata* is near-absent. Benthic foraminifera, after reaching high abundance around 30.30 m, maintained relatively high concentrations.

4.2. O and C stable isotopes

The main downcore feature of the $\delta^{18}O_{G.ruber}$ trend was an abrupt decrease at the base of the Sapropel deposition that corresponds to the laminated unit (Figs. 2 and 3). Throughout the sapropel unit, $\delta^{18}O$ values are generally low. However, it is worth mentioning that $\delta^{18}O$ values began to decrease just before dark-like sediments. Similar decreasing trends of the values were detected in the $\delta^{13}C$ records of *G. bulloides* and *B. marginata*, with the last one culminating just after the above-mentioned peak of $\delta^{18}O_{G.\ ruber}$. Decrease in $\delta^{13}C$ started well before the of $\delta^{18}O_{G.\ ruber}$ decrease though.

4.3. Geochemistry

Total organic carbon (TOC) concentration exhibited a small increment before the S5 unit followed by a rapid increase, particularly in the laminated unit (Fig. 2; up to ca. 1.2%). TOC values were relatively high throughout the S5 and then decreased to pre-sapropel values outside the dark-like sediments (ca. 0.3%). All redox sensitive elements (Mo, U, Sb) displayed a similar trend as observed for the TOC although each element showed its own differences reflecting the different behaviour under variable redox conditions during the sapropel S5 deposition. For example, Mo is rather high in the laminated unit while the U was relatively high throughout the event. Sb values started increasing before the laminated unit and reached the maximum values in the early phase of S5. The enrichment factors for individual elements followed the same downcore trends. Elemental ratios for sediment texture and provenance, ln(Zr/Rb) and Mg/Al_2O_3, exhibited a similar trend; before and after the S5 unit were relatively high while values decreased within the sapropel S5 unit. Alkenone-based SST showed a general increase (about 8 °C) before and during the S5 unit while the SST values decreased only after the S5 event. The SST did not show any sharp changes across the time period investigated but rather a constant increase.

5. Discussion

5.1. Abrupt shutdown of the north Adriatic dense water during MIS5e

In the Northern Adriatic, surface sea cooling in winter during cold Bora events generates a dense and oxygen-rich water mass (Northern Adriatic Dense Water, NAdDW). This dense plume then moves southward following the general circulation prior to cascading off the shelf in early spring to contribute to the Eastern Mediterranean Deep Water formation (Chiggiato et al., 2016; Langone et al., 2016; Vilibić and Supić, 2005). PRAD1-2 borehole is located on the path of this dense plume that travels confined along the western Adriatic shelf due to the Coriolis force (Marini et al., 2016). Regional models indicate that the mean propagation speed of dense water currents over the shelf during intense events (e.g., 2012) can reach up to 40–50 cm/s (Janeković et al., 2014). In this study, we used Zr/Rb and MgO/Al_2O_3 ratios to infer variations in the bottom water energy and sediment source, respectively, that in the modern system are both regulated by the NAdDW intensity. Zirconium is present in heavy minerals and, because they are resistant to physical/chemical weathering, it is commonly associated with the coarse-grained fraction of siliciclastic sediments (Fralick and Kronberg, 1997; Pettijohn, 1941). Rubidium, instead, is widespread in fine-grained particles, including K-rich clay minerals and K-feldspars (Dypvik and Harris, 2001; Fralick and Kronberg, 1997). Thus, the Zr/Rb ratio varies according to the sediment texture and in particular with the sortable fraction of siliciclastic material that, in turn, is a proxy of bottom current energy (McCave et al., 1995; Wu et al., 2020). In addition, as the source of the NAdDW is located in a region characterized by a relatively large input of dolomite-rich sediments supplied by local rivers draining the

Eastern Alps (Amorosi et al., 2022), changes in the MgO/Al_2O_3 ratio provide further information about the north-to-south connections and sediment transport mechanisms regulated by the NAdDW.

During MIS5e, Zr/Rb and MgO/Al_2O_3 in PRAD1-2 displayed a sharp drop that started ca. 128.8 ka BP and lasted until ca. 122 ka BP (Fig. 4a and b). Overall, this suggests a millennial-scale decrease of the bottom water energy coupled with a change in the source of sediment that became less influenced by the Northern Adriatic domain. We can thus infer that, for about 6 kyrs, the NAdDW experienced a severe reduction with no signs of recovery. We used piece-wise linear regression to identify the break points (Fig. 5b) and concluded that the change was relatively abrupt taking place in 0.67 ± 0.22 kyrs. Even considering the upper limit error associated with the age model framework, our results clearly contrast with the idea that the deposition of sapropels near glacial terminations requires a slow shutdown of the thermohaline forcing lasting several millennia. In particular, Grimm et al. (2015) have suggested that for sapropel S1 – and extended this interpretation to Quaternary sapropels – the anoxia required a long prelude of deep-water stagnation driven by the post-glacial inflow of relatively fresh deglacial Atlantic waters entering through Gibraltar. In their work, Grimm et al. (2015) have used the isotopic geochemistry of planktic and epi-benthic and planktic foraminifera to support their modelling effort and infer changes in the ventilation rate. They interpreted the isotopic shift in $\delta^{13}C$ towards negative values as a sign of progressive stagnation since the end of the Last Glacial Maximum in response to sea level rise.

By contrast, our reconstruction of the NAdDW activity suggests no evident cause-effect relationships between sea level rise (Fig. 4 a,b) and dense water formation (Fig. 4c). Yet, the $\delta^{13}C$ of *G. bulloides* and *B. marginata* throughout Termination II exhibited a long negative trend (we used *B. marginata* as epi-benthic foraminifera were discontinuous; Fig. 4 d,e) that would suggest a progressive stagnation throughout the penultimate deglaciation. Other evidence that supports pre-conditioning include anomalies in TOC, redox-sensitive elements (Mo, U and Sb) and deep infaunal species that exhibited an increase before MIS5e (Figs. 4f, 5e-i). However, changes in all these deoxygenation proxies were rather small compared to the abrupt increase observed later on when the dense water formation suddenly dropped. Finally, other diagnostic signs of deoxygenation like the number of benthic foraminifera - apparently not affected during the pre-sapropel period - exhibited a rapid change only with the sudden NAdDW reduction (Fig. 5h).

We argue that these pre-sapropel conditions were essentially the result of increased nutrient availability in response to sea level rise (Ausín et al., 2015). Specifically, the inflow of nutrient-rich Atlantic waters probably enhanced primary productivity and organic matter export to the seabed. This ultimately decreased pore-water oxygen concentration despite the well-ventilated conditions generating mild-suboxic conditions at the seabed. Subsequently, bottom waters reached critical oxygen deficiency conditions exclusively when the dense water formation in the Northern Adriatic experienced the abrupt reduction documented in our study. Another evidence that goes against a long prelude of deep-water stagnation is the high coherence between our shallow-water record and LC21 sediment core from the Aegean Sea (1522 m water depth; Fig. 4f). Specifically, in a scenario of millennial-scale prelude to stagnation, the shallow-water environment should necessarily lag beyond the deep system. Instead, the TOC content over time exhibited substantially the same trend in both shallow and deep domains.

In summary, despite some evidence for an early stagnation starting millennia prior to MIS5e, our NAdDW proxies rule out the reduction of the dense water formation as an important factor during this early phase. More likely the nutrient supply, driven by the inflow of Atlantic waters following the penultimate glacial termination, played a central role in the early deoxygenation. The reason why $\delta^{13}C$ anomalies of benthic and planktic foraminifera lead the stagnation by several millennia is not fully understood; yet, our collective evidence does not recommend the use of $\delta^{13}C$ in foraminifera over the shelf as an exclusive tracer of ventilation. Given the general correlation between sea level rise and $\delta^{13}C$ of foraminifera, we rather suspect that the post-glacial flooding of the Adriatic shelf combined with the modification of the water column structure in a relatively shallow setting might have affected the dissolved inorganic carbon pool (Bird et al., 2010; Woodruff and Savin, 1985) and ultimately the $\delta^{13}C$ fingerprint.

5.2. *Mechanisms driving the abrupt NAdDW reduction*

Freshening of the Eastern Mediterranean is a fundamental prerequisite that drives the sapropel formation (Rohling et al., 2015). The freshwater input promotes stagnation preconditioning surface waters offsetting the winter cooling. In addition, the fresh water can stimulates primary productivity that, in turn, increases the oxygen consumption at the seabed (De Lange et al., 2008; Rossignol-Strick et al., 1982). Changes in the surface water salinity at the onset of sapropel S5 have been recorded across the whole Eastern Mediterranean as isotopically depleted $\delta^{18}O$ values of *G. ruber* (Fig. 4g) (Cane et al., 2002; Capotondi et al., 2006; Vergnaud-Grazzini et al., 1977). There are three major sources of freshwater documented in the literature: African monsoons, W-E Atlantic perturbations and retreating ice sheets (this latter input via either Gibraltar strait or land routing e.g., Fennoscandian ice sheet, through the Black Sea) (Amies et al., 2019; Hennekam et al., 2014; Milner et al., 2012; Soulet et al., 2013; Toucanne et al., 2015). In addition, potential freshening in the NAdDW source area might have occurred during the rapid retreat of the ice caps on European Alps and the Dinaric Alps (Moseley et al., 2015). The input via African borderlands, following the orbitally-driven northward migration of the African monsoons, is commonly accepted as at the main contribution to stagnation as it is capable of changing the salinity of Levantine Intermediate Waters (Osborne et al., 2010; van der Meer et al., 2007; Weldeab et al., 2014) and, in turn, the density of surface waters over the Adriatic shelf where the dense water forms (Tesi et al., 2017).

Winter cooling during Bora events is another key aspect affecting the NAdDW formation. Today the seasonal heat loss driven by cold and dry winds is far the most important forcing that regulates the dense water formation in the Northern Adriatic (Bensi et al., 2013; Bonaldo et al., 2016; Janeković et al., 2014; Vilibić and Supić, 2005). Across MIS6 and MIS5e, the $SST_{alkenones}$ in the Adriatic exhibited a general increase with values generally lower than the Aegean Sea, which is consistent with today's climate (Fig. 4j). However, as the dense water formation in the Northern Adriatic takes a few weeks in winter during events of rapid heat loss (Janeković et al., 2014), we question whether the annual SST obtained via alkenones is indeed a representative index to infer past NAdDW dynamics. Indeed, recent studies carried out in the modern Adriatic setting suggest that alkenones record mean annual temperatures without an evident seasonal bias (Leider et al., 2010). We thus compared our reconstruction with the January temperature derived from pollen data in MD04-2845 core collected in the Bay of Biscay that reflects the general southern Europe climate (Salonen et al., 2021) (Fig. 4k). The overall picture suggests mean temperatures of January at the onset of MIS5e above 0 °C. This temperature is much warmer than the characteristic temperatures observed in typical winters distinctive for an extensive NAdDW formation (i.e., well below 0 °C: e.g. 2012; Janeković et al., 2014). According to the pollen data from MD04-2845, before MIS5e winter temperatures were cold enough to promote the dense water formation consistent with our NAdDW reconstruction. Other pollen-based winter temperatures further east from the Ohrid lake (western Balkans; Sinopoli et al., 2019) suggest an analogous abrupt change at the onset of MIS5e, supporting the hypothesis that temperature changes in the coldest months of the year ultimately affected the NAdDW formation together with the freshwater supply to the LIW source area. Similarly, rapid change in pollen assemblages with the development of warm-temperate forests was observed in the Po plain along the Western Adriatic coast (Amorosi et al., 2004). Overall, the

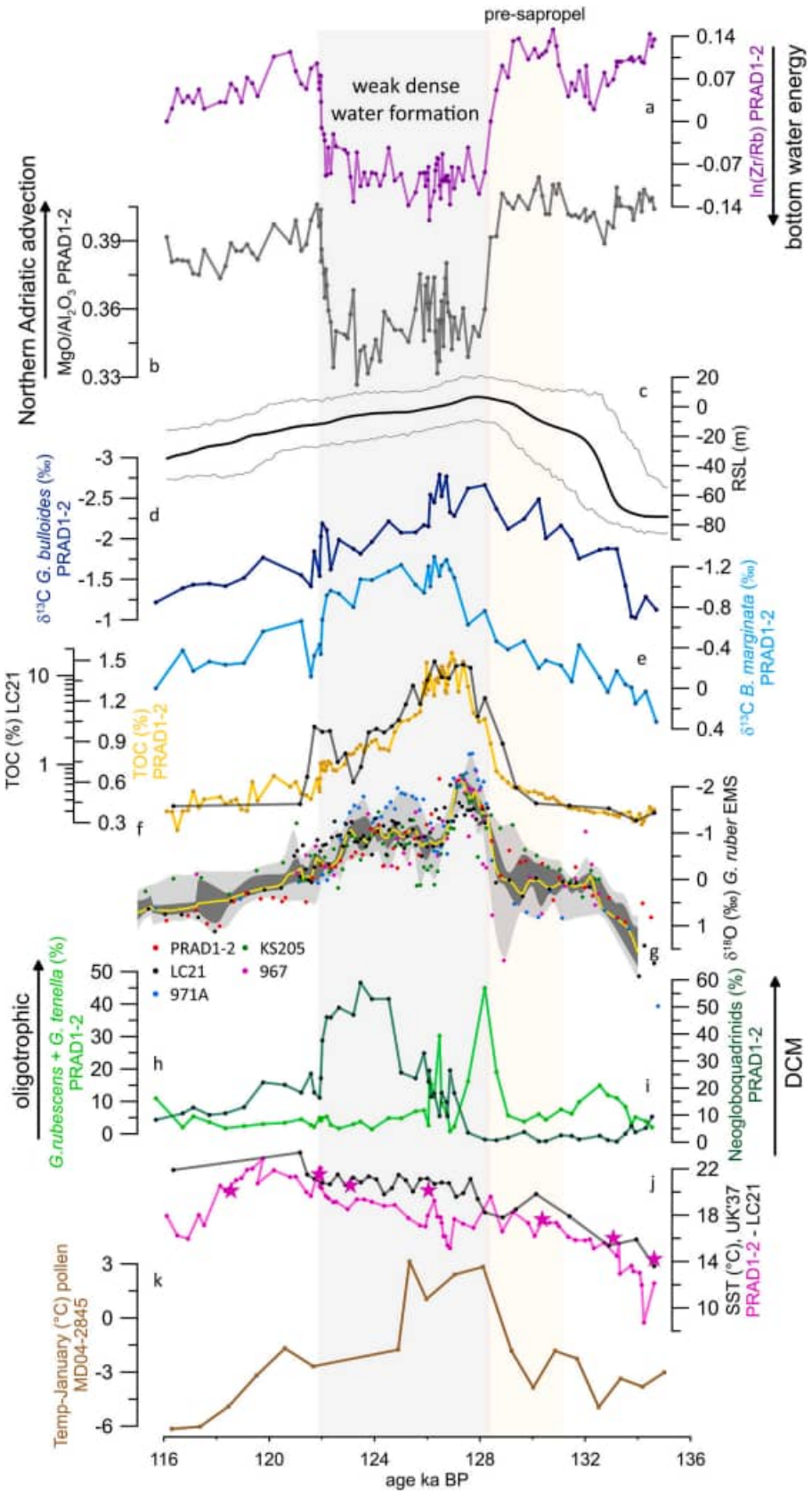

(caption on next page)

Fig. 4. (a) Zr/Rb ratio proxy for bottom water energy; (b) MgO/Al_2O_3 ratio proxy for sediment source; (c) relative sea level (RSL, m) after Grant et al., 2012; (d, e) $\delta^{13}C$ (‰) of *G. bulloides* and *B. marginata*; (f) total organic carbon (TOC, %) of LC21 (Marino et al., 2007) and PRAD1-2 (this study); (g) $\delta^{18}O$ (‰) *G. ruber* of PRAD1-2 (this study), LC21, ODP971A, KS205 and ODP967 (Amies et al., 2019). Eastern Mediterranean $\delta^{18}O$ stack of *G. ruber*: median (solid yellow line), 68% and 95% confidence limits (shaded grey envelopes) (this study); (h) abundance (%) of *G. rubenscens* and *G. tenella*; (i) abundance (%) of Neogloboquadrinids; (j) alkenone-based Sea Surface Temperature (SST, °C) of PRAD1-2 (this study) and LC21 (Marino et al., 2007), stars show previous low resolution data for PRAD1-2 from Piva et al., 2008a; (k) pollen-based air temperature (°C) in January (MD04-2845; Salonen et al., 2021). Grey area shows the sapropel S5 and light pink indicates the pre-sapropel period.

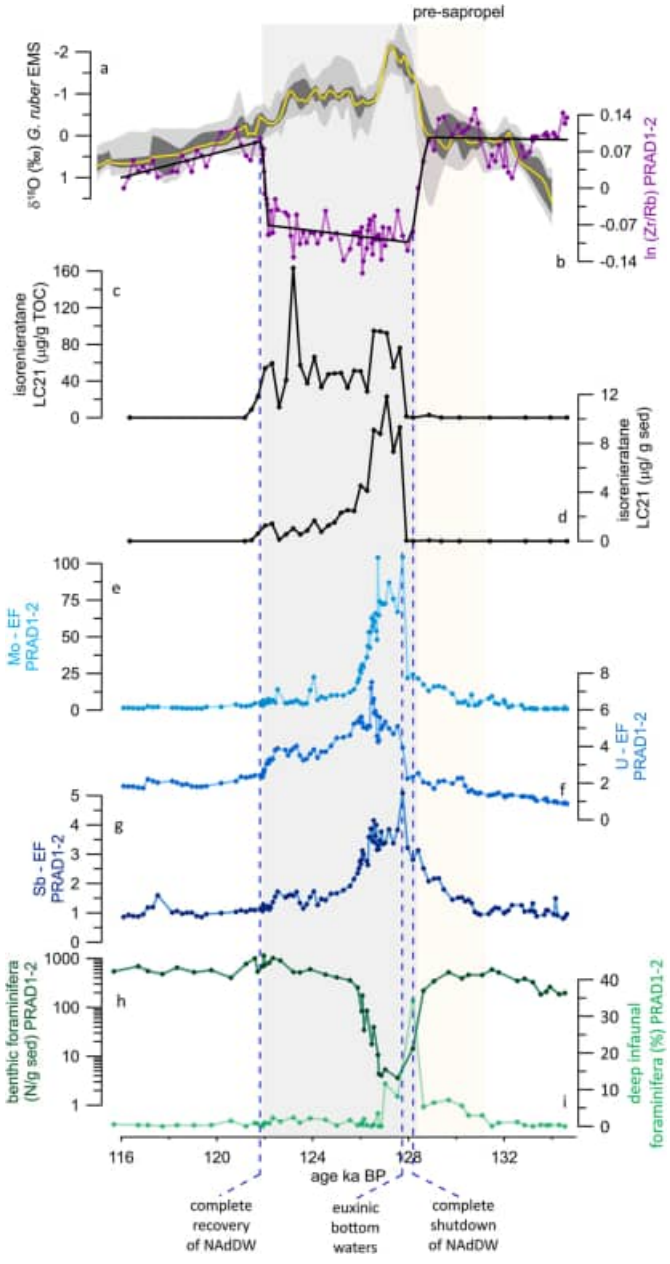

Fig. 5. (a) Eastern Mediterranean $\delta^{18}O$ stack of *G. ruber*: median (solid yellow line), 68% and 95% confidence limits (shaded grey envelopes) (this study); (b) Zr/Rb ratio proxy for bottom water energy (solid line shows the piece-wise linear regression analysis; (c, d) TOC- and sediment-normalized isorenieratane concentrations in LC21, respectively (Marino et al., 2007); (e) Mo enrichment factor (Mo-EF); (f) U enrichment factor (U-EF); (g) Sb enrichment factor (Sb-EF); (h) benthic foraminifera concentration (N/g); (i) abundance (%) of deep infaunal benthic taxa. Grey area shows the sapropel S5 and light pink indicates the pre-sapropel period. Colored symbols and lines refer to new data presented in this study, otherwise literature data for LC21 are in black.

thermal profile of the MIS5e of the EPICA stack well correlates with the $\delta^{18}O$ *G. ruber*. The early phase of S5 (pre-sapropel) corresponds to the rising-limb of the warming responses of precession and half-precession, with a final acceleration (centennial scale) determined by the co-phasing of sun-related suborbital cycles (Masson-Delmotte et al., 2006; Viaggi, 2021; Yin and Berger, 2012). Overall, this supports our results indicating that the shutdown of the NAdDW production occurred within few centuries.

In summary, we suggest that the centennial-scale variability in the thermohaline forcing reconstructed in the Northern Adriatic was primarily caused by the combination of freshening of surface waters with winter temperature increasing (Fig. 4g,k) that mutually hampered the formation of the NAdDW (Dirksen and Meijer, 2020). Similarly, the complete resumption of the NAdDW 6 millennia after its shutdown occurred only when the surface salinity and the winter temperature turned back to pre-sapropel values. According to Zr/Rb and MgO/Al_2O_3 data, as observed for the S5 onset, the full recovery of the NAdDW was a centennial-scale process (ca. 0.35 ± 0.1 kyrs) (Fig. 5a), yet apparently quicker than the initial shutdown.

Planktic foraminifera provided further insights into the changes occurred in the water column. For instance, the grazing group of Neogloboquadrinids are commonly associated with the Deep Chlorophyll Maximum (DCM) and thus their relative abundance informs about the position of the nutricline that develops in stratified water column conditions (Fairbanks and Wiebe, 1980; Rohling and Gieskes, 1989; Sierro et al., 2003). However, at the early onset of S5 the presence of Neogloboquadrinids is negligible (Fig. 4i) despite the expected stratification caused by warming and freshening. We argue that the stratification was indeed pronounced at the onset of the deoxygenation event to a point that the nutricline was positioned well below the euphotic zone. Water turbidity might also have contributed by shoaling the base of the euphotic zone (Grelaud et al., 2012). A nutricline positioned far from the euphotic zone at the onset of S5 is also suggested by the high abundance of *G. rubescens* and *G. tenella* that are common species in warm and nutrient-starve surface waters (Avnaim-Katav et al., 2020; Jentzen et al., 2018; Jonkers and Kučera, 2015) (Fig. 4h). SEM images further support the general oligotrophic conditions with the laminated pattern at the onset of S5 entirely constituted by coccolith and coccospheres of *Umbellosphaera tenuis* and *Discosphaera tubifera* that are typical of warm and oligotrophic environment (Chen et al., 2007; Godrijan et al., 2018) (Fig. 6). To some extent this contrasts with coeval diatom-rich mats observed in the S5 unit further east (Kemp et al., 1999) while it is consistent with the development of oligotrophic surface waters during the early S5 in the Urania Basin (Corselli et al., 2002). We also argue that the shallow setting (i.e., continental shelf) might have hampered the development of favourable conditions for autotrophs blooming in the lower euphotic zone (Corselli et al., 2002) in the early phase of S5. The development of a stable DCM - as suggested by the high abundance of Neogloboquadrinids - occurred only later in the second half of S5 (Fig. 4i). Shoaling of the pycnocline within the euphotic zone might have been caused by changes in surface water salinity and regional atmospheric cooling that mutually lowered the degree of stratification and ultimately favoured the development of a stable DCM.

5.3. *Variability within the sapropel S5 unit*

Overall, the anomalies for all deoxygenation proxies (trace metals and benthic foraminifera) followed the general millennial-scale

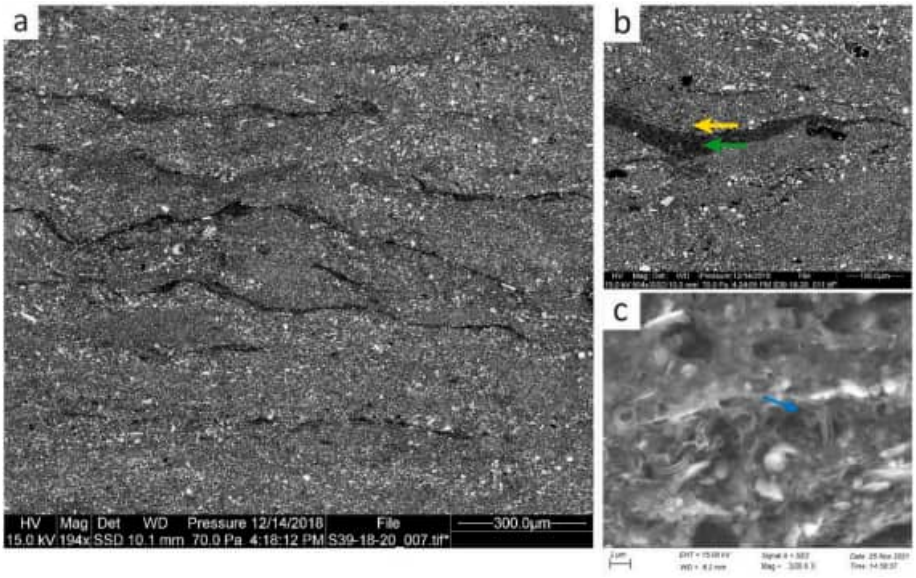

Fig. 6. SEM images of a thin section within the lower sapropel S5 unit (section 39 18–20 cm, ca. 127.3 kyrs BP). (a) wavy pinch-and-swell laminae and probably minor disruption by meiofaunal burrowers; (b) distinct lamina compositions. Clastic and biogenic laminae are highlighted with yellow and green arrows, respectively. The clastic laminae is mainly constituted by clay, bioclasts, and mineralogenic detritus, while the biogenic lamina is entirely constituted by coccolith and coccospheres; (c) close-up of the laminae constituted by coccolith and coccospheres with examples of well-preserved coccosphere *Emiliania huxleyi* (blue arrow). The latter suggests particle settling in a small time span and no/very weak bottom current.

stagnation reconstructed with Zr/Rb and MgO/Al_2O_3 ratios (Fig. 5). Yet, despite the protracted weakening of the NAdDW for about six millennia, the deoxygenation exhibited ample variability within the sapropel unit with an early phase particularly deoxygenated followed by a gradual recovery. The piece-wise linear regression of the Zr/Rb ratio indeed suggests an early phase with a particularly weak NAdDW followed by a gentle recovery (Fig. 5a). However, this trend does not seem sufficient to justify the difference observed across the sapropel unit. We thus envision that other factors must have necessarily taken place to explain the two phases within the deoxygenation event.

The onset of S5 is virtually anoxic despite the presence of a few benthic foraminifera (ca. 5–10 specimens) tolerant to oxygen-poor conditions (Fig. 5h and i). This is consistent with the redox sensitive elements (Mo, U, Sb) that displayed typical values observed within modern permanent oxygen minimum zones (Bennett and Canfield, 2020; Fig. 5e–g). Yet, each redox sensitive elements exhibited its own variability within the S5 unit which reflects the different chemical behaviour of each metal species under variable redox conditions (Algeo and Tribovillard, 2009; Emerson and Huested, 1991; Herath et al., 2017). The excess of Mo in particular is a diagnostic sign for an early phase particularly reducing and rich in dissolved H_2S (euxinic) that allows the conversion of molybdate oxyanion into particle reactive thiomolybdates followed by authigenic Mo deposition via sulfidized humic trapping and Fe–S phases (Algeo and Tribovillard, 2009; Tribovillard et al., 2012). According to Mo anomalies, the abrupt onset of euxinic conditions at 127.76 ± 0.1 ka BP over the Adriatic shelf lagged about 340 yrs behind the shutdown of the NAdDW (128.1 ± 0.1 ka BP) (Fig. 5b,e). Yet, benthic foraminifera responded more rapidly to changes in ventilation, exhibiting a marked drop in abundance (from ca. 700 to 20 N/g) at 128.1 ± 0.1 ka BP (Fig. 5h). When compared with the Aegean Sea (Marino et al., 2007), the sediment-normalized concentration of isorenieratane in LC21 indeed confirms the abrupt development of euxinic conditions in shallow-waters during the early phase of S5 in phase with our Mo record (Fig. 5d). This allowed the proliferation of isorenieratane-producing green-sulphur bacteria in the euphotic zone. These organisms, in fact, perform photosynthesis with reduced sulphur and light implying euxinic and virtually oxygen-free conditions in the upper water column (Repeta, 1993; Sinninghe Damsté et al., 1993, 2001). After the S5 onset, the sediment-normalized concentrations of isorenieratane in LC21 progressively decrease within the sapropelite unit consistent with the Mo record in PRAD1-2.

However, the TOC-normalized concentration of isorenieratane in LC21 – as opposed to the sediment-normalized values discussed above – exhibited a millennial-scale and persistent anomaly similar to Zr/Rb and MgO/Al_2O_3 records in PRAD1-2 (Fig. 5c). To reconcile our results with the difference in isorenieratene trends depending on the normalization used, we infer that the S5 deposition consisted of an early phase with virtually absent convection and LIW influence followed by another period in which the deep water convection was still highly reduced while oxygen concentrations in shallow/upper-intermediate waters showed their early signs of recovery. It is possible that this intermediate water mass corresponded to a weak LIW that was formed as the surface salinity increased across the EMS ($\delta^{18}O$ of *G. ruber*, Fig. 5a). In addition, cooling of the mean winter temperature in the second part of S5 at regional level (Frogley et al., 1999; Rioual et al., 2001; Salonen et al., 2021) likely favoured the mixing of surface waters without, however, generating important events of NAdDW formation, but providing enough oxygen to support benthic life over the Adriatic shelf. This phase of gradual recovery and resumption of surface circulation indeed follows the global temperature reduction after the climax determined mainly by both precession and half-precession in-phase cooling hemicycles (Viaggi, 2021). Yet, alkenone-derived SST (Fig. 4j) did not suggest a significant cooling as reported by pollen records (Fig. 4k) which could be a sign of an incomplete representation of the winter mixing season as previously discussed or that the increased salinity was indeed the major driver. Evidence of surface water re-oxygenation are also evident in the Aegean Sea (LC21) where the extent of the surface euxinic layer likely changed from permanent to seasonal. This, in turn, affected the absolute concentration of isorenieratane in sediments yet maintaining a general condition of weak dense water formation (Fig. 5d). In fact, the presence of isorenieratane in sediments, even in small concentrations regardless its normalization, necessarily indicates an oxygen-free environment as these organisms are strictly anaerobic (Repeta, 1993; Sinninghe Damsté et al., 1993, 2001). Overall, this scenario would reconcile the trends observed in TOC-normalized isorenieratane data (Fig. 5c) and our NAdDW proxies (Zr/Rb and MgO/Al_2O_3) (Fig. 4a and b and 5b).

The second phase of the sapropel over the Adriatic shelf can thus be considered moderately deoxygenated like a suboxic environment (Tyson and Pearson, 1991). The different redox conditions that experienced S5 over time fully elucidates the contrasting trends observed for U-EF and Mo-EF (Algeo and Tribovillard, 2009; Chiu et al., 2022; Tribovillard et al., 2012) (Fig. 5e and f). Under reducing conditions with H_2S expanding in the water column (i.e. S5 onset), rates of Mo uptake substantially exceed those of U, resulting in a marked increase of the Mo/U ratio in sediments (Algeo and Tribovillard, 2009; Tribovillard et al., 2012). Instead, under suboxic conditions, U is scavenged preferentially over Mo because U(VI) is efficiently reduced at the Fe(II)–Fe(III) redox boundary across the sediment-water interface (Algeo and Tribovillard, 2009; Tribovillard et al., 2012). This explains why the U record exhibited moderately low values despite the high authigenic Mo accumulation at the onset of S5 while in the second phase, when Mo decreased, U anomalies remained relatively stable. The two phases within the S5 unit is also supported by the distribution of Neogloboquadrinids (Fig. 4i) as previously discussed that suggested a general reorganization of the water column, possibly reflecting the shoaling of the nutricline and the development of a stable DCM only in the second part of the event.

To the best of our knowledge, PRAD1-2 is the first highly-resolved shallow-water record of S5 and therefore we do not have additional reconstructions from shallow settings to compare with. However, in support to our hypothesis, signs of the partial recovery of oxygen in shallow/intermediate waters in the second half of S5 have been recorded in the benthic foraminifera from the Levantine Basin. Here, Schmiedl et al. (2003) have analysed the distribution of benthic foraminifera in two records from 1433 to 2158 m and found signs of benthic fauna recovery in the shallower core during the second half of the event. By contrast, the deep system remained anoxic until the full resumption of convection. In general, the whole deep EMS remained fully anoxic for several millennia without showing any evidence of re-oxygenation until the dense water formation fully recovered (Capotondi et al., 2006; Chiu et al., 2022). Schmiedl et al. (2003) argued that cooling recorded in the second half of the S5 event (Frogley et al., 1999; Rioual et al., 2001) may have favoured the formation of dense water capable to plunge to intermediate- and potentially greater depth (Fig. 4k). Our results indicate that, despite the general increase of surface salinities and cooling during the second half of S5, Northern Adriatic waters never became dense enough for the complete resumption of the NAdDW justifying this apparent decoupling between physical forcing and redox conditions.

6. Comparison with future scenarios

In this section we compare our outcomes with modelling exercise to infer the extent of thermohaline shutdown. This comparison is a qualitative exercise implying similar conditions relative to the modern Adriatic, especially as far as the sea level is concerned that can be considered comparable in first-order approximation. There are only two regional models that have assessed the future oxygen evolution of the Mediterranean Sea until 2100 of which only one has modelled the long-term oxygen loss (Powley et al., 2016; Reale et al., 2022). Both models agree on the fact that anoxia is rather unlikely to occur in the Eastern and Western Mediterranean Sea (EMS and WMS) by 2100, even considering the *business as usual* scenario RCP 8.5 (Reale et al., 2022). Anoxia instead could only develop after several centuries of weak convection (75% and 85% thermohaline reduction in WMS and EMS, respectively) and exclusively in the deep EMS (<500 m) while surface (0–200 m) and intermediate waters (200–500 m) remain fully oxygenated in all simulations (Powley et al., 2016). Models also indicate that for the long-term deoxygenation, the decrease of the dense water formation plays a first-order control whereas temperature-driven dissolution and microbial oxygen uptake are less relevant in the long term (Powley et al., 2016).

Our observational evidence from the Adriatic shelf agree on the impact of the dense water formation over centennial-time scales – thus different from the millennial-scale preconditioning proposed in earlier publications – although the general picture is rather different. Specifically, euxinic conditions with virtually absence of benthic life developed ca. 900 years since the beginning of the NAdDW slowdown and ca. 350 years upon reaching the new steady low level of ventilation (see sections 4.1 and 4.2). Although this centennial-scale mechanism is somehow consistent with the long-term deoxygenation trend reproduced by models, none of the simulations predicted an anoxic shallow-water environment as reported in our study (Powley et al., 2016; Reale et al., 2022). Because the long-term deoxygenation reproduced by models is based on a 85% reduction of the dense water production for the EMS compared to modern conditions (Powley et al., 2016; Somot et al., 2006), we suggest the virtually complete shutdown of the NAdDW at the onset of S5 to justify the anoxia development in shallow-waters (<200 m). This is especially true considering the absence of strong evidence for enhanced primary productivity in our dataset that makes the physical forcing as the main driver. Thus, although the severity of the future deoxygenation driven by climate change appears quite far from the expression of a natural climate event like the S5, our results imply that any significant deviation from today's expected reduction in the dense water formation (Somot et al., 2006) will necessarily drive the deoxygenation towards more severe conditions as showed in this study.

7. Summary and conclusions

Our study provides novel evidence that severe deoxygenation extended over the shallow Adriatic shelf (<200 m) during sapropel S5 and, thus, highlights the large-scale expression of this anoxic event (Fig. 7). We used the geochemical fingerprint of sedimentary material to assess north-to-south connection (MgO/Al_2O_3) and bottom water energy (Zr/Rb) that collectively reflect the export of dense water coming from the Northern Adriatic shelf (Fig. 4 a,b). Our results indicate that the shutdown of the NAdDW production at the onset of MIS5e occurred within a few centuries (Fig. 4 a,b). This highly contrasts with the hypothesis of a long prelude (millennial-scale), assumed to be necessary to develop stagnation in the EMS (Grimm et al., 2015). According to our NAdDW proxies, the shutdown lasted for about 6 kyrs (from ca. 128 to 122 ka BP) followed by a rapid recovery. In this study, we suggest that the NAdDW shutdown was the result of winter temperature increase combined with the large-scale freshening of the surface EMS (Fig. 3). A few centuries after the onset of stagnation, bottom water became euxinic while benthic foraminifera virtually disappeared. The overall pattern observed at the beginning of S5 in the Adriatic shelf follows the temporal trend reconstructed further east in the deep Aegean Sea (Fig. 4). This highlights the lack of substantial leads/lags and further rules out the millennial-scale precondition as this latter would have necessarily resulted in a shallow-water setting lagging behind the deep sea. After an early phase with strong reducing conditions that lasted ca. 2 kyrs, the second part of S5 experienced a gradual recovery marked by geochemical and ecological characteristics typical of a suboxic environment (Fig. 5). We envision that atmospheric cooling and decrease in salinity observed in the second part of S5 likely promoted the mixing of surface waters without, however, generating intense dense water cascading events over this period that lasted ca. 4 kyrs.

Overall, our results highlight the added value of studying shallow-water sapropel deposits. First of all, working on the margin we reconstructed the dense water formation and export of oxygen to an unprecedented level. In addition, shallow-water sapropels provide a unique opportunity to disentangle physical forcing (i.e., cascading) and geochemical/biological processes (i.e., sapropel) within the same archive circumventing the evident limitations of merging together different records affected by inevitable age uncertainties. Finally, although the possibility for the EMS to experience in the future an event similar to S5 seems indeed remote (Powley et al., 2016; Reale et al., 2022), in the event that the anticipated weakening of the EMS

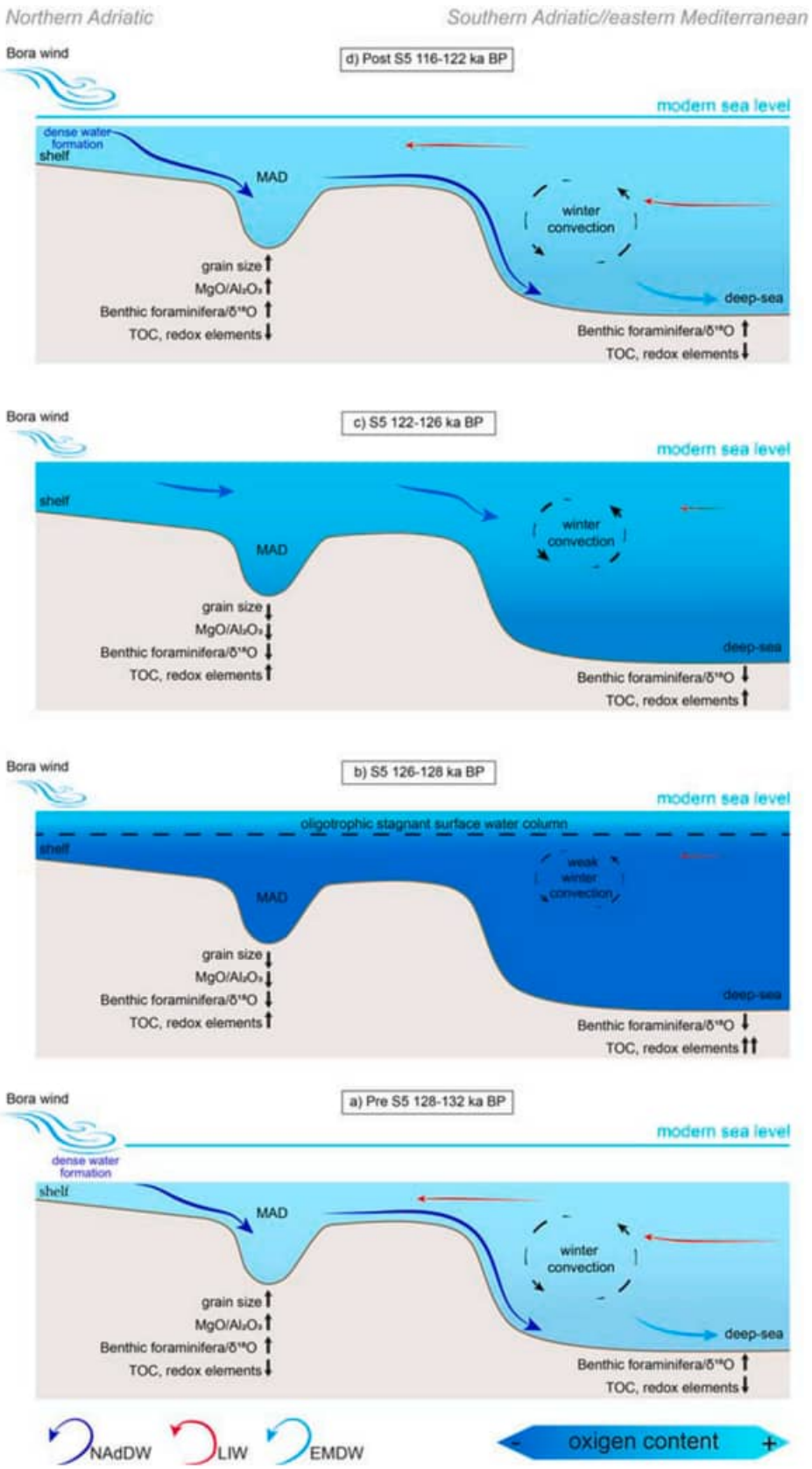

(caption on next page)

Fig. 7. Cartoon showing the different phases of the S5 deposition in shallow and deep systems. Dark blue arrows show the Northern Adriatic Dense Water (NAdDW), the red arrows show the Levantine Intermediate Water (LIW) and light blue arrow indicate the Eastern Mediterranean Deep Water (EMDW). Black arrows show the relative changes of proxies investigated in this study that vary as a function of the degree of ventilation. Shaded blue color shows the relative oxygen content. a) pre-sapropel S5: fully oxygenated condition with regular thermohaline circulation. b) S5 onset: strong anoxia driven by change in surface water salinity (freshening) and warming of winter temperatures. Under these conditions the thermohaline forcing virtually shutdowns. c) Second part of S5: partial recovery of the winter mixing because of the overall winter temperature cooling without, however, full recovery of the NAdDW. Relative increase of the oxygen content. d) post-sapropel S5: full recovery of the NAdDW formation and fully oxygenated conditions.

thermohaline forcing is worse than presently anticipated, the deoxygenation will likely occur in a few centuries and it will affect the shallow-water system as documented in our study.

Declaration of competing interest

The authors declare that they have no known competing financial interests or personal relationships that could have appeared to influence the work reported in this paper.

Data availability

Data are available as supplementary material

Acknowledgements

This study is part of the GREAT project funded by Eni S.p.A. Upstream Research and Technological Innovation. All data presented in this study can be find in the Supplementary section.

Appendix A. Supplementary data

Supplementary data to this article can be found online at https://doi.org/10.1016/j.qsa.2023.100134.

References

Adloff, F., Somot, S., Sevault, F., Jordà, G., Aznar, R., Déqué, M., Herrmann, M., Marcos, M., Dubois, C., Padorno, E., Alvarez-Fanjul, E., Gomis, D., 2015. Mediterranean Sea response to climate change in an ensemble of twenty first century scenarios. Clim. Dynam. 45, 2775–2802. https://doi.org/10.1007/s00382-015-2507-3.

Algeo, T.J., Tribovillard, N., 2009. Environmental analysis of paleoceanographic systems based on molybdenum–uranium covariation. Chem. Geol. 268, 211–225. https://doi.org/10.1016/j.chemgeo.2009.09.001.

Amies, J.D., Rohling, E.J., Grant, K.M., Rodríguez-Sanz, L., Marino, G., 2019. Quantification of african monsoon runoff during last interglacial sapropel S5. Paleoceanogr. Paleoclimatol. 34, 1487–1516. https://doi.org/10.1029/2019PA003652.

Amorosi, A., Colalongo, M.L., Fiorini, F., Fusco, F., Pasini, G., Vaiani, S.C., Sarti, G., 2004. Palaeogeographic and palaeoclimatic evolution of the Po Plain from 150-ky core records. Global Planet. Change 40 (1–2), 55–78.

Amorosi, A., Sammartino, I., Dinelli, E., Campo, B., Guercia, T., Trincardi, F., Pellegrini, C., 2022. Provenance and sediment dispersal in the Po-Adriatic source-to-sink system unraveled by bulk-sediment geochemistry and its linkage to catchment geology. Earth Sci. Rev. 234, 104202 https://doi.org/10.1016/j.earscirev.2022.104202.

Argentino, C., Lugli, F., Cipriani, A., Conti, S., Fontana, D., 2019. A deep fluid source of radiogenic Sr and highly dynamic seepage conditions recorded in Miocene seep carbonates of the northern Apennines (Italy). Chem. Geol. 522, 135–147. https://doi.org/10.1016/j.chemgeo.2019.05.029.

Ausín, B., Flores, J.-A., Sierro, F.-J., Bárcena, M.-A., Hernández-Almeida, I., Francés, G., Gutiérrez-Arnillas, E., Martrat, B., Grimalt, J.O., Cacho, I., 2015. Coccolithophore productivity and surface water dynamics in the Alboran Sea during the last 25 kyr. Palaeogeogr. Palaeoclimatol. Palaeoecol. 418, 126–140. https://doi.org/10.1016/j.palaeo.2014.11.011.

Avnaim-Katav, S., Herut, B., Rahav, E., Katz, T., Weinstein, Y., Alkalay, R., Berman-Frank, I., Zlatkin, O., Almogi-Labin, A., 2020. Sediment trap and deep sea coretop sediments as tracers of recent changes in planktonic foraminifera assemblages in the southeastern ultra-oligotrophic Levantine Basin. Deep Sea Res. Part II Top. Stud. Oceanogr. 171, 104669 https://doi.org/10.1016/j.dsr2.2019.104669.

Barmawidjaja, D.M., Jorissen, F.J., Puskaric, S., Van Der Zwaan, G.J., 1992. Microhabitat selection by benthic foraminifera in the northern adriatic sea. J. Foraminifer. Res. 22, 297–317. https://doi.org/10.2113/gsjfr.22.4.297.

Bennett, W.W., Canfield, D.E., 2020. Redox-sensitive trace metals as paleoredox proxies: a review and analysis of data from modern sediments. Earth Sci. Rev. 204, 103175 https://doi.org/10.1016/j.earscirev.2020.103175.

Bensi, M., Cardin, V., Rubino, A., Notarstefano, G., Poulain, P.M., 2013. Effects of winter convection on the deep layer of the Southern Adriatic Sea in 2012: effects of strong shelf convection. J. Geophys. Res. Oceans 118, 6064–6075. https://doi.org/10.1002/2013JC009432.

Bird, M.I., Austin, W.E.N., Wurster, C.M., Fifield, L.K., Mojtahid, M., Sargeant, C., 2010. Punctuated eustatic sea-level rise in the early mid-Holocene. Geology 38, 803–806. https://doi.org/10.1130/G31066.1.

Bonaldo, D., Benetazzo, A., Bergamasco, A., Campiani, E., Foglini, F., Sclavo, M., Trincardi, F., Carniel, S., 2016. Interactions among Adriatic continental margin morphology, deep circulation and bedform patterns. Mar. Geol. 375, 82–98. https://doi.org/10.1016/j.margeo.2015.09.012.

Bourne, A.J., Albert, P.G., Matthews, I.P., Trincardi, F., Wulf, S., Asioli, A., Blockley, S.P.E., Keller, J., Lowe, J.J., 2015. Tephrochronology of core PRAD 1-2 from the Adriatic Sea: insights into Italian explosive volcanism for the period 200–80 ka. Quat. Sci. Rev. 116, 28–43. https://doi.org/10.1016/j.quascirev.2015.03.006.

Bulian, F., Kouwenhoven, T.J., Jiménez-Espejo, F.J., Krijgsman, W., Andersen, N., Sierro, F.J., 2022. Impact of the Mediterranean-Atlantic connectivity and the late Miocene carbon shift on deep-sea communities in the Western Alboran Basin. Palaeogeogr. Palaeoclimatol. Palaeoecol. 589, 110841 https://doi.org/10.1016/j.palaeo.2022.110841.

Cane, T., Rohling, E.J., Kemp, A.E.S., Cooke, S., Pearce, R.B., 2002. High-resolution stratigraphic framework for Mediterranean sapropel S5: defining temporal relationships between records of Eemian climate variability. Palaeogeogr. Palaeoclimatol. Palaeoecol. 183, 87–101. https://doi.org/10.1016/S0031-0182(01)00461-8.

Capotondi, L., Principato, M.S., Morigi, C., Sangiorgi, F., Maffioli, P., Giunta, S., Negri, A., Corselli, C., 2006. Foraminiferal variations and stratigraphic implications to the deposition of sapropel S5 in the eastern Mediterranean. Palaeogeogr. Palaeoclimatol. Palaeoecol. 235, 48–65. https://doi.org/10.1016/j.palaeo.2005.09.023.

Chen, Y.L., Chen, H.-Y., Chung, C.-W., 2007. Seasonal variability of coccolithophore abundance and assemblage in the northern South China Sea. Deep Sea Res. Part II Top. Stud. Oceanogr. 54, 1617–1633. https://doi.org/10.1016/j.dsr2.2007.05.005.

Chiggiato, J., Bergamasco, A., Borghini, M., Falcieri, F.M., Falco, P., Langone, L., Miserocchi, S., Russo, A., Schroeder, K., 2016. Dense-water bottom currents in the southern adriatic sea in spring 2012. Mar. Geol. 375, 134–145. https://doi.org/10.1016/j.margeo.2015.09.005.

Chiu, C.F., Sweere, T.C., Clarkson, M.O., de Souza, G.F., Hennekam, R., Vance, D., 2022. Co-variation systematics of uranium and molybdenum isotopes reveal pathways for descent into euxinia in Mediterranean sapropels. Earth Planet Sci. Lett. 585, 117527 https://doi.org/10.1016/j.epsl.2022.117527.

Clarkson, M.O., Hennekam, R., Sweere, T.C., Andersen, M.B., Reichart, G.-J., Vance, D., 2021. Carbonate associated uranium isotopes as a novel local redox indicator in oxidatively disturbed reducing sediments. Geochem. Cosmochim. Acta 311, 12–28. https://doi.org/10.1016/j.gca.2021.07.025.

Corselli, C., Principato, M.S., Maffioli, P., Crudeli, D., 2002. Changes in planktonic assemblages during sapropel S5 deposition: evidence from Urania Basin area, eastern Mediterranean. Paleoceanography 17 (3), 1-1.

Cutmore, A., Ausín, B., Maslin, M., Eglinton, T., Hodell, D., Muschitiello, F., Menviel, L., Haghipour, N., Martrat, B., Margari, V., Tzedakis, P.C., 2022. Abrupt intrinsic and extrinsic responses of southwestern Iberian vegetation to millennial-scale variability over the past 28 ka. J. Quat. Sci. 37, 420–440. https://doi.org/10.1002/jqs.3392.

De Lange, G.J., Thomson, J., Reitz, A., Slomp, C.P., Speranza Principato, M., Erba, E., Corselli, C., 2008. Synchronous basin-wide formation and redox-controlled preservation of a Mediterranean sapropel. Nat. Geosci. 1, 606–610. https://doi.org/10.1038/ngeo283.

De Rijk, S., Troelstra, S.R., Rohling, E.J., 1999. Benthic foraminiferal distribution in the Mediterranean Sea. J. Foraminifer. Res. 29, 93–103. https://doi.org/10.2113/gsjfr.29.2.93.

De Stigter, H.C., Jorissen, F.J., Van der Zwaan, G.J., 1998. Bathymetric distribution and microhabitat partitioning of live (Rose Bengal stained) benthic foraminifera along a shelf to bathyal transect in the southern Adriatic Sea. J. Foraminifer. Res. 28, 40–65.

Dirksen, J.P., Meijer, P., 2020. The mechanism of sapropel formation in the Mediterranean Sea: insight from long-duration box model experiments. Clim. Past 16, 933–952. https://doi.org/10.5194/cp-16-933-2020.

Dypvik, H., Harris, N.B., 2001. Geochemical facies analysis of fine-grained siliciclastics using Th/U, Zr/Rb and (Zr+Rb)/Sr ratios. Chem. Geol. 181, 131–146. https://doi.org/10.1016/S0009-2541(01)00278-9.

Emerson, S.R., Huested, S.S., 1991. Ocean anoxia and the concentrations of molybdenum and vanadium in seawater. Mar. Chem. 34, 177–196. https://doi.org/10.1016/0304-4203(91)90002-E.

Fairbanks, R.G., Wiebe, P.H., 1980. Foraminifera and chlorophyll maximum: vertical distribution, seasonal succession, and paleoceanographic significance. Science 209, 1524–1526.

Ferranti, L., Antonioli, F., Mauz, B., Amorosi, A., Dai Pra, G., Mastronuzzi, G., Verrubbi, V., 2006. Markers of the last interglacial sea-level high stand along the coast of Italy: tectonic implications. Quat. Int. 145, 30–54.

Fralick, P.W., Kronberg, B.I., 1997. Geochemical discrimination of clastic sedimentary rock sources. Sediment. Geol. 113, 111–124. https://doi.org/10.1016/S0037-0738(97)00049-3.

Frogley, M.R., Tzedakis, P.C., Heaton, T.H.E., 1999. Climate variability in northwest Greece during the last interglacial. Science 285, 1886–1889. https://doi.org/10.1126/science.285.5435.1886.

Godrijan, J., Young, J.R., Marić Pfannkuchen, D., Precali, R., Pfannkuchen, M., 2018. Coastal zones as important habitats of coccolithophores: a study of species diversity, succession, and life-cycle phases. Limnol. Oceanogr. 63, 1692–1710. https://doi.org/10.1002/lno.10801.

Grant, K.M., Amarathunga, U., Amies, J.D., Hu, P., Qian, Y., Penny, T., Rodriguez-Sanz, L., Zhao, X., Heslop, D., Liebrand, D., Hennekam, R., Westerhold, T., Gilmore, S., Lourens, L.J., Roberts, A.P., Rohling, E.J., 2022. Organic carbon burial in Mediterranean sapropels intensified during Green Sahara Periods since 3.2 Myr ago. Commun. Earth Environ 3, 11. https://doi.org/10.1038/s43247-021-00339-9.

Grant, K.M., Rohling, E.J., Bar-Matthews, M., Ayalon, A., Medina-Elizalde, M., Ramsey, C.B., Satow, C., Roberts, A.P., 2012. Rapid coupling between ice volume and polar temperature over the past 150,000 years. Nature 491, 744–747. https://doi.org/10.1038/nature11593.

Grelaud, M., Marino, G., Ziveri, P., Rohling, E.J., 2012. Abrupt shoaling of the nutricline in response to massive freshwater flooding at the onset of the last interglacial sapropel event: shoaling of the nutricline during S5. Paleoceanography 27. https://doi.org/10.1029/2012PA002288 n/a-n/a.

Grimm, R., Maier-Reimer, E., Mikolajewicz, U., Schmiedl, G., Müller-Navarra, K., Adloff, F., Grant, K.M., Ziegler, M., Lourens, L.J., Emeis, K.-C., 2015. Late glacial initiation of Holocene eastern Mediterranean sapropel formation. Nat. Commun. 6, 7099. https://doi.org/10.1038/ncomms8099.

Hennekam, R., Jilbert, T., Schnetger, B., de Lange, G.J., 2014. Solar forcing of Nile discharge and sapropel S1 formation in the early to middle Holocene eastern Mediterranean. Paleoceanography 29, 343–356. https://doi.org/10.1002/2013PA002553.

Herath, I., Vithanage, M., Bundschuh, J., 2017. Antimony as a global dilemma: geochemistry, mobility, fate and transport. Environ. Pollut. 223, 545–559. https://doi.org/10.1016/j.envpol.2017.01.057.

Hernández-Almeida, I., Bárcena, M.A., Flores, J.A., Sierro, F.J., Sanchez-Vidal, A., Calafat, A., 2011. Microplankton response to environmental conditions in the Alboran Sea (Western Mediterranean): one year sediment trap record. Mar. Micropaleontol. 78, 14–24. https://doi.org/10.1016/j.marmicro.2010.09.005.

Herrmann, M., Estournel, C., Déqué, M., Marsaleix, P., Sevault, F., Somot, S., 2008. Dense water formation in the Gulf of Lions shelf: impact of atmospheric interannual variability and climate change. Continent. Shelf Res. 28, 2092–2112. https://doi.org/10.1016/j.csr.2008.03.003.

Janeković, I., Mihanović, H., Vilibić, I., Tudor, M., 2014. Extreme cooling and dense water formation estimates in open and coastal regions of the Adriatic Sea during the winter of 2012. J. Geophys. Res. Oceans 119, 3200–3218. https://doi.org/10.1002/2014JC009865.

Jentzen, A., Schönfeld, J., Schiebel, R., 2018. Assessment of the effect of increasing temperature on the ecology and assemblage structure of modern planktic foraminifers in the caribbean and surrounding seas. J. Foraminifer. Res. 48, 251–272. https://doi.org/10.2113/gsjfr.48.3.251.

Jonkers, L., Kučera, M., 2015. Global analysis of seasonality in the shell flux of extant planktonic Foraminifera. Biogeosciences 12, 2207–2226. https://doi.org/10.5194/bg-12-2207-2015.

Jorissen, F.J., 1999. Benthic foraminiferal successions across late quaternary mediterranean sapropels. Mar. Geol. 153, 91–101. https://doi.org/10.1016/S0025-3227(98)00088-7.

Jorissen, F.J., 1988. Benthic Foraminifera from the Adriatic Sea: Principles of Phenotypic Variation. Utrecht University.

Kemp, A.E.S., Pearce, R.B., Koizumi, I., Pike, J., Rance, S.J., 1999. The role of mat-forming diatoms in the formation of Mediterranean sapropels. Nature 398, 57–61. https://doi.org/10.1038/18001.

Kwiatkowski, L., Torres, O., Bopp, L., Aumont, O., Chamberlain, M., Christian, J.R., Dunne, J.P., Gehlen, M., Ilyina, T., John, J.G., Lenton, A., Li, H., Lovenduski, N.S., Orr, J.C., Palmieri, J., Santana-Falcón, Y., Schwinger, J., Séférian, R., Stock, C.A., Tagliabue, A., Takano, Y., Tjiputra, J., Toyama, K., Tsujino, H., Watanabe, M., Yamamoto, A., Yool, A., Ziehn, T., 2020. Twenty-first century ocean warming, acidification, deoxygenation, and upper-ocean nutrient and primary production decline from CMIP6 model projections. Biogeosciences 17, 3439–3470. https://doi.org/10.5194/bg-17-3439-2020.

Langone, L., Conese, I., Miserocchi, S., Boldrin, A., Bonaldo, D., Carniel, S., Chiggiato, J., Turchetto, M., Borghini, M., Tesi, T., 2016. Dynamics of particles along the western margin of the Southern Adriatic: processes involved in transferring particulate matter to the deep basin. Mar. Geol. 375, 28–43. https://doi.org/10.1016/j.margeo.2015.09.004.

Leider, A., Hinrichs, K.-U., Mollenhauer, G., Versteegh, G.J.M., 2010. Core-top calibration of the lipid-based U37K′ and TEX86 temperature proxies on the southern Italian shelf (SW Adriatic Sea, Gulf of Taranto). Earth Planet Sci. Lett. 300, 112–124. https://doi.org/10.1016/j.epsl.2010.09.042.

Leoni, L., Saitta, M., 1976. Determination of yttrium and niobium on standard silicate rocks by X-ray fluorescence analyses. X Ray Spectrom. 5, 29–30. https://doi.org/10.1002/xrs.1300050107.

Mallo, M., Ziveri, P., Mortyn, P.G., Schiebel, R., Grelaud, M., 2017. Low planktic foraminiferal diversity and abundance observed in a spring 2013 west–east Mediterranean Sea plankton tow transect. Biogeosciences 14, 2245–2266. https://doi.org/10.5194/bg-14-2245-2017.

Marini, M., Maselli, V., Campanelli, A., Foglini, F., Grilli, F., 2016. Role of the Mid-Adriatic deep in dense water interception and modification. Mar. Geol. 375, 5–14. https://doi.org/10.1016/j.margeo.2015.08.015.

Marino, G., Rohling, E.J., Rijpstra, W.I.C., Sangiorgi, F., Schouten, S., Damsté, J.S.S., 2007. Aegean Sea as driver of hydrographic and ecological changes in the eastern Mediterranean. Geology 35, 675. https://doi.org/10.1130/G23831A.1.

Maselli, V., Trincardi, F., Cattaneo, A., Ridente, D., Asioli, A., 2010. Subsidence pattern in the central Adriatic and its influence on sediment architecture during the last 400 kyr. J. Geophys. Res. 115, B12106 https://doi.org/10.1029/2010JB007687.

Masson-Delmotte, V., Kageyama, M., Braconnot, P., Charbit, S., Krinner, G., Ritz, C., Guilyardi, E., Jouzel, J., Abe-Ouchi, A., Crucifix, M., 2006. Past and future polar amplification of climate change: climate model intercomparisons and ice-core constraints. Clim. Dynam. 26, 513–529.

McCave, I.N., Manighetti, B., Robinson, S.G., 1995. Sortable silt and fine sediment size/composition slicing: parameters for palaeocurrent speed and palaeoceanography. Paleoceanography 10, 593–610. https://doi.org/10.1029/94PA03039.

Milner, A.M., Collier, R.E.L., Roucoux, K.H., Müller, U.C., Pross, J., Kalaitzidis, S., Christanis, K., Tzedakis, P.C., 2012. Enhanced seasonality of precipitation in the Mediterranean during the early part of the Last Interglacial. Geology 40, 919–922. https://doi.org/10.1130/G33204.1.

Moseley, G.E., Spötl, C., Cheng, H., Boch, R., Min, A., Edwards, R.L., 2015. Termination-II interstadial/stadial climate change recorded in two stalagmites from the north European Alps. Quat. Sci. Rev. 127, 229–239.

Müller, P.J., Kirst, G., Ruhland, G., von Storch, I., Rosell-Melé, A., 1998. Calibration of the alkenone paleotemperature index U37K′ based on core-tops from the eastern South Atlantic and the global ocean (60°N-60°S). Geochem. Cosmochim. Acta 62, 1757–1772. https://doi.org/10.1016/S0016-7037(98)00097-0.

Murray, J.W., 2006. Ecology and Applications of Benthic Foraminifera, first ed. Cambridge University Press. https://doi.org/10.1017/CBO9780511535529.

Muschitiello, F., D'Andrea, W.J., Schmittner, A., Heaton, T.J., Balascio, N.L., deRoberts, N., Caffee, M.W., Woodruff, T.E., Welten, K.C., Skinner, L.C., Simon, M. H., Dokken, T.M., 2019. Deep-water circulation changes lead North Atlantic climate during deglaciation. Nat. Commun. 10, 1272. https://doi.org/10.1038/s41467-019-09237-3.

Muschitiello, F., O'Regan, M., Martens, J., West, G., Gustafsson, Ö., Jakobsson, M., 2020. A new 30 000-year chronology for rapidly deposited sediments on the Lomonosov Ridge using bulk radiocarbon dating and probabilistic stratigraphic alignment. Geochronology 2, 81–91. https://doi.org/10.5194/gchron-2-81-2020.

Osborne, A.H., Marino, G., Vance, D., Rohling, E.J., 2010. Eastern Mediterranean surface water Nd during Eemian sapropel S5: monitoring northerly (mid-latitude) versus southerly (sub-tropical) freshwater contributions. Quat. Sci. Rev. 29, 2473–2483.

Pellegrini, C., Asioli, A., Bohacs, K.M., Drexler, T.M., Feldman, H.R., Sweet, M.L., Maselli, V., Rovere, M., Gamberi, F., Valle, G.D., Trincardi, F., 2018. The Late Pleistocene Po River lowstand wedge in the Adriatic Sea: controls on architecture variability and sediment partitioning. Mar. Petrol. Geol. 96, 16–50. https://doi.org/10.1016/j.marpetgeo.2018.03.002.

Pellegrini, C., Maselli, V., Gamberi, F., Asioli, A., Bohacs, K.M., Drexler, T.M., Trincardi, F., 2017. How to make a 350-m-thick lowstand systems tract in 17,000 years: the Late Pleistocene Po River (Italy) lowstand wedge. Geology 45, 327–330. https://doi.org/10.1130/G38848.1.

Pellegrini, C., Tesi, T., Schieber, J., Bohacs, K.M., Rovere, M., Asioli, A., Nogarotto, A., Trincardi, F., 2021. Fate of terrigenous organic carbon in muddy clinothems on continental shelves revealed by stratal geometries: insight from the Adriatic sedimentary archive. Global Planet. Change 203, 103539. https://doi.org/10.1016/j.gloplacha.2021.103539.

Pettijohn, F.J., 1941. Persistence of heavy minerals and geologic age. J. Geol. 49, 610–625. https://doi.org/10.1086/624992.

Piva, A., Asioli, A., Andersen, N., Grimalt, J.O., Schneider, R.R., Trincardi, F., 2008a. Climatic cycles as expressed in sediments of the PROMESS1 borehole PRAD1-2, central Adriatic, for the last 370 ka: 2. Paleoenvironmental evolution: evolution of PROMESS1 borehole PRAD1-2. G-cubed 9. https://doi.org/10.1029/2007GC001785 n/a-n/a.

Piva, A., Asioli, A., Schneider, R.R., Trincardi, F., Andersen, N., Colmenero-Hidalgo, E., Dennielou, B., Flores, J.-A., Vigliotti, L., 2008b. Climatic cycles as expressed in sediments of the PROMESS1 borehole PRAD1-2, central Adriatic, for the last 370 ka: 1. Integrated stratigraphy: stratigraphy of PROMESS1 borehole PRAD1-2. G-cubed 9. https://doi.org/10.1029/2007GC001713 n/a-n/a.

Powley, H.R., Krom, M.D., Van Cappellen, P., 2016. Circulation and oxygen cycling in the Mediterranean Sea: sensitivity to future climate change: oxygen cycling in the Mediterranean Sea. J. Geophys. Res. Oceans 121, 8230–8247. https://doi.org/10.1002/2016JC012224.

Pujol, C., Grazzini, C.V., 1995. Distribution patterns of live planktic foraminifers as related to regional hydrography and productive systems of the Mediterranean Sea. Mar. Micropaleontol. 25, 187–217. https://doi.org/10.1016/0377-8398(95)00002-I.

Reale, M., Cossarini, G., Lazzari, P., Lovato, T., Bolzon, G., Masina, S., Solidoro, C., Salon, S., 2022. Acidification, deoxygenation, and nutrient and biomass declines in a warming Mediterranean Sea. Biogeosciences 19, 4035–4065. https://doi.org/10.5194/bg-19-4035-2022.

Repeta, D.J., 1993. A high resolution historical record of Holocene anoxygenic primary production in the Black Sea. Geochem. Cosmochim. Acta 57, 4337–4342. https://doi.org/10.1016/0016-7037(93)90334-S.

Ridente, D., Trincardi, F., Piva, A., Asioli, A., 2009. The combined effect of sea level and supply during Milankovitch cyclicity: evidence from shallow-marine δ18O records

and sequence architecture (Adriatic margin). Geology 37, 1003–1006. https://doi.org/10.1130/G25730A.1.
Ridente, D., Trincardi, F., Piva, A., Asioli, A., Cattaneo, A., 2008. Sedimentary response to climate and sea level changes during the past ~400 ka from borehole PRAD1-2 (Adriatic margin): sedimentary response to climate and sea level change. G-cubed 9. https://doi.org/10.1029/2007GC001783 n/a-n/a.
Rigual-Hernández, A.S., Sierro, F.J., Bárcena, M.A., Flores, J.A., Heussner, S., 2012. Seasonal and interannual changes of planktic foraminiferal fluxes in the Gulf of Lions (NW Mediterranean) and their implications for paleoceanographic studies: two 12-year sediment trap records. Deep-Sea Res. Part A Oceanogr. Res. Pap. 66, 26–40. https://doi.org/10.1016/j.dsr.2012.03.011.
Rioual, P., Andrieu-Ponel, V., Rietti-Shati, M., Battarbee, R.W., de Beaulieu, J.-L., Cheddadi, R., Reille, M., Svobodova, H., Shemesh, A., 2001. High-resolution record of climate stability in France during the last interglacial period. Nature 413, 293–296. https://doi.org/10.1038/35095037.
Rivalenti, G., Mazzucchelli, M., Laurora, A., Ciuffi, S.I.A., Zanetti, A., Vannucci, R., Cingolani, C.A., 2004. The backarc mantle lithosphere in Patagonia, South America. J. South Am. Earth Sci. 17, 121–152. https://doi.org/10.1016/j.jsames.2004.05.009.
Rohling, E.J., Gieskes, W.W.C., 1989. Late Quaternary changes in Mediterranean intermediate water density and formation rate. Paleoceanography 4, 531–545. https://doi.org/10.1029/PA004i005p00531.
Rohling, E.J., Marino, G., Grant, K.M., 2015. Mediterranean climate and oceanography, and the periodic development of anoxic events (sapropels). Earth Sci. Rev. 143, 62–97. https://doi.org/10.1016/j.earscirev.2015.01.008.
Rontani, J.-F., Wakeham, S.G., Prahl, F.G., Vaultier, F., Volkman, J.K., 2011. Analysis of trace amounts of alkenones in complex environmental samples by way of NaBH4/NaBD4 reduction and silylation. Org. Geochem. 42, 1299–1307. https://doi.org/10.1016/j.orggeochem.2011.09.004.
Rossignol-Strick, M., Nesteroff, W., Olive, P., Vergnaud-Grazzini, C., 1982. After the deluge: Mediterranean stagnation and sapropel formation. Nature 295, 105–110. https://doi.org/10.1038/295105a0.
Salonen, J.S., Sánchez-Goñi, M.F., Renssen, H., Plikk, A., 2021. Contrasting northern and southern European winter climate trends during the Last Interglacial. Geology 49, 1220–1224. https://doi.org/10.1130/G49007.1.
Schiebel, R., Hemleben, C., 2017. Planktic Foraminifers in the Modern Ocean. Springer Berlin Heidelberg, Berlin, Heidelberg. https://doi.org/10.1007/978-3-662-50297-6.
Schieber, J., 2013. 13 SEM Observations on Ion-Milled Samples of Devonian Black Shales from Indiana and New York: the Petrographic Context of Multiple Pore Types.
Schimmelmann, A., Riese, D.J., Schieber, J., 2015. Fast and economical sampling and resin-embedding technique for small cores of unconsolidated, fine-grained sediment. In: Proceedings of the 2015 Pacific Climate (PACLIM) Workshop. Asilomar Conference Grounds, Pacific Grove, CA, USA, pp. 8–11.
Schmidtko, S., Stramma, L., Visbeck, M., 2017. Decline in global oceanic oxygen content during the past five decades. Nature 542, 335–339. https://doi.org/10.1038/nature21399.
Schmiedl, G., De Bovée, F., Buscail, R., Charrière, B., Hemleben, C., Medernach, L., Picon, P., 2000. Trophic control of benthic foraminiferal abundance and microhabitat in the bathyal Gulf of Lions, western Mediterranean Sea. Mar. Micropaleontol. 40, 167–188. https://doi.org/10.1016/S0377-8398(00)00038-4.
Schmiedl, G., Mitschele, A., Beck, S., Emeis, K.-C., Hemleben, C., Schulz, H., Sperling, M., Weldeab, S., 2003. Benthic foraminiferal record of ecosystem variability in the eastern Mediterranean Sea during times of sapropel S5 and S6 deposition. Palaeogeogr. Palaeoclimatol. Palaeoecol. 190, 139–164. https://doi.org/10.1016/S0031-0182(02)00603-X.
Sen Gupta, B.K., 2003. Modern Foraminifera. Springer Netherlands, Dordrecht. https://doi.org/10.1007/0-306-48104-9.
Sessford, E.G., Jensen, M.F., Tisserand, A.A., Muschitiello, F., Dokken, T., Nisancioglu, K. H., Jansen, E., 2019. Consistent fluctuations in intermediate water temperature off the coast of Greenland and Norway during Dansgaard-Oeschger events. Quat. Sci. Rev. 223, 105887 https://doi.org/10.1016/j.quascirev.2019.105887.
Sierro, F.J., Flores, J.A., Francés, G., Vazquez, A., Utrilla, R., Zamarreño, I., Erlenkeuser, H., Barcena, M.A., 2003. Orbitally-controlled oscillations in planktic communities and cyclic changes in western Mediterranean hydrography during the Messinian. Palaeogeogr. Palaeoclimatol. Palaeoecol. 190, 289–316. https://doi.org/10.1016/S0031-0182(02)00611-9.
Sinninghe Damsté, J.S., Schouten, S., van Duin, A.C.T., 2001. Isorenieratene derivatives in sediments: possible controls on their distribution. Geochem. Cosmochim. Acta 65, 1557–1571. https://doi.org/10.1016/S0016-7037(01)00549-X.
Sinninghe Damsté, J.S., Wakeham, S.G., Kohnen, M.E.L., Hayes, J.M., de Leeuw, J.W., 1993. A 6,000–year sedimentary molecular record of chemocline excursions in the Black Sea. Nature 362, 827–829. https://doi.org/10.1038/362827a0.
Sinopoli, G., Peyron, O., Masi, A., Holtvoeth, J., Francke, A., Wagner, B., Sadori, L., 2019. Pollen-based temperature and precipitation changes in the Ohrid Basin (western Balkans) between 160 and 70 ka. Clim. Past 15, 53–71. https://doi.org/10.5194/cp-15-53-2019.
Somot, S., Sevault, F., Déqué, M., 2006. Transient climate change scenario simulation of the Mediterranean Sea for the twenty-first century using a high-resolution ocean circulation model. Clim. Dynam. 27, 851–879. https://doi.org/10.1007/s00382-006-0167-z.
Soulet, G., Ménot, G., Bayon, G., Rostek, F., Ponzevera, E., Toucanne, S., Lericolais, G., Bard, E., 2013. Abrupt drainage cycles of the fennoscandian ice sheet. Proc. Natl. Acad. Sci. USA 110, 6682–6687. https://doi.org/10.1073/pnas.1214676110.
Tesi, T., Asioli, A., Minisini, D., Maselli, V., Dalla Valle, G., Gamberi, F., Langone, L., Cattaneo, A., Montagna, P., Trincardi, F., 2017. Large-scale response of the Eastern Mediterranean thermohaline circulation to African monsoon intensification during sapropel S1 formation. Quat. Sci. Rev. 159, 139–154. https://doi.org/10.1016/j.quascirev.2017.01.020.
Tesi, T., Muschitiello, F., Mollenhauer, G., Miserocchi, S., Langone, L., Ceccarelli, C., Panieri, G., Chiggiato, J., Nogarotto, A., Hefter, J., Ingrosso, G., Giglio, F., Giordano, P., Capotondi, L., 2021. Rapid atlantification along the fram strait at the beginning of the 20th century. Sci. Adv. 7, eabj2946 https://doi.org/10.1126/sciadv.abj2946.
Toucanne, S., Angue Minto'o, C.M., Fontanier, C., Bassetti, M.-A., Jorry, S.J., Jouet, G., 2015. Tracking rainfall in the northern Mediterranean borderlands during sapropel deposition. Quat. Sci. Rev. 129, 178–195. https://doi.org/10.1016/j.quascirev.2015.10.016.
Tribovillard, N., Algeo, T.J., Baudin, F., Riboulleau, A., 2012. Analysis of marine environmental conditions based onmolybdenum–uranium covariation—applications to Mesozoic paleoceanography. Chem. Geol. 324–325, 46–58. https://doi.org/10.1016/j.chemgeo.2011.09.009.
Tyson, R.V., Pearson, T.H., 1991. Modern and ancient continental shelf anoxia: an overview. Geol. Soc. Lond. Spec. Publ. 58, 1–24.
van der Meer, M.T.J., Baas, M., Rijpstra, W.I.C., Marino, G., Rohling, E.J., Sinninghe Damsté, J.S., Schouten, S., 2007. Hydrogen isotopic compositions of long-chain alkenones record freshwater flooding of the Eastern Mediterranean at the onset of sapropel deposition. Earth Planet Sci. Lett. 262, 594–600. https://doi.org/10.1016/j.epsl.2007.08.014.
Vergnaud-Grazzini, C., Ryan, W.B., Cita, M.B., 1977. Stable isotopic fractionation, climate change and episodic stagnation in the eastern Mediterranean during the late Quaternary. Mar. Micropaleontol. 2, 353–370.
Viaggi, P., 2021. Quantitative impact of astronomical and sun-related cycles on the Pleistocene climate system from Antarctica records. Quat. Sci. Adv. 4, 100037.
Vilibić, I., Šepić, J., Proust, N., 2013. Weakening thermohaline circulation in the adriatic sea. Clim. Res. 55, 217–225. https://doi.org/10.3354/cr01128.
Vilibić, I., Supić, N., 2005. Dense water generation on a shelf: the case of the Adriatic Sea. Ocean Dynam. 55, 403–415. https://doi.org/10.1007/s10236-005-0030-5.
Weldeab, S., Menke, V., Schmiedl, G., 2014. The pace of East African monsoon evolution during the Holocene: weldeab et. AL.; east african monsoon evolution. Geophys. Res. Lett. 41, 1724–1732. https://doi.org/10.1002/2014GL059361.
Woodruff, F., Savin, S.M., 1985. δ13C values of Miocene Pacific benthic foraminifera: correlations with sea level and biological productivity. Geology 13, 119. https://doi.org/10.1130/0091-7613(1985)13<119:CVOMPB>2.0.CO;2.
Wu, L., Wilson, D.J., Wang, R., Yin, X., Chen, Z., Xiao, W., Huang, M., 2020. Evaluating Zr/Rb ratio from XRF scanning as an indicator of grain-size variations of glaciomarine sediments in the southern ocean. G-cubed 21. https://doi.org/10.1029/2020GC009350.
Yin, Q.Z., Berger, A., 2012. Individual contribution of insolation and CO 2 to the interglacial climates of the past 800,000 years. Clim. Dynam. 38, 709–724.
Zimmermann, T., Von Der Au, M., Reese, A., Klein, O., Hildebrandt, L., Pröfrock, D., 2020. Substituting HF by HBF_4 – an optimized digestion method for multi-elemental sediment analysis *via* ICP-MS/MS. Anal. Methods 12, 3778–3787. https://doi.org/10.1039/D0AY01049A.